This article was downloaded by:
On: *21 January 2011*
Access details: *Access Details: Free Access*
Publisher *Taylor & Francis*
Informa Ltd Registered in England and Wales Registered Number: 1072954 Registered office: Mortimer House, 37-41 Mortimer Street, London W1T 3JH, UK

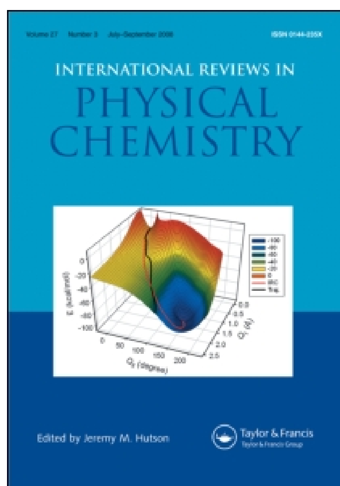

International Reviews in Physical Chemistry
Publication details, including instructions for authors and subscription information:
http://www.informaworld.com/smpp/title~content=t713724383

The application of molecular dynamics to the study of plasma-surface interactions: CF*_x* with silicon

F. Gou[a]; A. W. Kleyn[ab]; M. A. Gleeson[a]
[a] FOM-Institute for Plasma Physics Rijnhuizen, Edisonbaan 14, 3439 MN Nieuwegein, The Netherlands
[b] Gorlaeus Laboratories, Leiden Institute of Chemistry, 2300 RA Leiden, The Netherlands

To cite this Article Gou, F. , Kleyn, A. W. and Gleeson, M. A.(2008) 'The application of molecular dynamics to the study of plasma-surface interactions: CF*_x* with silicon', International Reviews in Physical Chemistry, 27: 2, 229 — 271
To link to this Article: DOI: 10.1080/01442350801928014
URL: http://dx.doi.org/10.1080/01442350801928014

PLEASE SCROLL DOWN FOR ARTICLE

Full terms and conditions of use: http://www.informaworld.com/terms-and-conditions-of-access.pdf

This article may be used for research, teaching and private study purposes. Any substantial or systematic reproduction, re-distribution, re-selling, loan or sub-licensing, systematic supply or distribution in any form to anyone is expressly forbidden.

The publisher does not give any warranty express or implied or make any representation that the contents will be complete or accurate or up to date. The accuracy of any instructions, formulae and drug doses should be independently verified with primary sources. The publisher shall not be liable for any loss, actions, claims, proceedings, demand or costs or damages whatsoever or howsoever caused arising directly or indirectly in connection with or arising out of the use of this material.

International Reviews in Physical Chemistry
Vol. 27, No. 2, April–June 2008, 229–271

Taylor & Francis
Taylor & Francis Group

The application of molecular dynamics to the study of plasma–surface interactions: CF_x with silicon

F. Gou[a], A. W. Kleyn[ab]* and M. A. Gleeson[a]

[a]*FOM-Institute for Plasma Physics Rijnhuizen, Edisonbaan 14, 3439 MN Nieuwegein, The Netherlands;* [b]*Gorlaeus Laboratories, Leiden Institute of Chemistry, 2300 RA Leiden, The Netherlands*

(*Received 3 December 2007; final version received 17 January 2008*)

In this paper, we provide an overview of the use of molecular dynamics for simulations involving energetic particles (Ar, F, and CF_x) interacting with silicon surfaces. The groups (including our own) that have performed this work are seeking to advance the fundamental understanding of plasma interactions at surfaces. Although this paper restricts itself largely to the systems bracketed above, the approach and general mechanisms involved are applicable to a much wider range of systems. Proper description of plasma-related systems generally requires a large number of atoms in order to correctly characterize the interactions. Consequently, the bulk of the present work, and the main focus of the text, is based on classical molecular dynamics. In MD simulations, one of the most critical considerations is the selection of the interatomic potential. For simulations involving silicon etching, the choice is typically made between the Stillinger–Weber and the Tersoff–Brenner potentials. An outline of the two potentials is given, including efforts that have been made to improve and optimize the potentials and their parameters. Subsequently, we focus on some of the practical details involved in establishing the simulation process and outline how various parameters (e.g. heat bath, relaxation time and cell size) influence the simulation results. These sections deal with the influences of the heat bath (application time, rising time), the time-step and total integration time of molecular trajectories, the relaxation of the sample (during and post-etching) and the sample size. The approach is essentially pedagogical in nature, and may be of interest to those less familiar with the techniques. To illustrate the type of results that can be produced we present a case study for 100 eV CF_3^+ interacting with a Si(100)-2×1 surface at different sample temperatures (100–800 K). The simulations reveal details of the change in etch rate, the F-turnover and the standing coverage of functional groups as a function of the temperature. Our primary interest is in studies with relevance for plasma–surface interactions. We discuss the general mechanisms that are most important in plasma–surface interactions and give an overview of some of the wide range of results that have been produced for various systems. The results presented illustrate that careful consideration must be given to the precise configuration of the plasma system. Numerous factors, including the chemical species, the energy and chemical mix of the incident particles and the surface composition and structure can play a crucial role in determining the net outcome of the interaction.

*Corresponding author. Email: A.W.Kleyn@rijnh.nl

ISSN 0144–235X print/ISSN 1366–591X online
© 2008 Taylor & Francis
DOI: 10.1080/01442350801928014
http://www.informaworld.com

Downloaded At: 15:50 21 January 2011

Contents

PAGE

1. Introduction 231
1.1. Experimental approaches 232
1.2. Theoretical approaches 232
1.2.1. *Ab initio* molecular dynamics 233
1.2.2. Classical molecular dynamics 234

2. Simulation methods 235
2.1. Classical MD simulations using empirical potentials 235
2.1.1. SW potential 235
2.1.2. Tersoff-Brenner potential 236
2.1.3. Improving the potentials 238
2.2. Sample preparation 239
2.3. Effects of the Simulation Method 241
2.3.1. Temperature control mechanism 241
2.3.1.1. Nosé-Hoover thermostat 242
2.3.1.2. Andersen thermostat 242
2.3.1.3. Berendsen thermostat 242
2.3.2. Thermostat parameters 243
2.3.2.1. Application time 243
2.3.2.2. Coupling strength 245
2.3.3. Simulation time-scale 247
2.3.3.1. Time-step 247
2.3.3.2. Integration time 248
2.3.3.3. Relaxation time 248
2.3.4. Cell size effect 249

3. Case study: surface temperature effects 250

4. Plasma-surface interactions 258
4.1. Mechanisms of PSI 258
4.2. Species effects 260
4.2.1. F Radical 261
4.2.2. Ar^+ ion 261
4.2.3. F^+ ion 261
4.2.4. CF_x^+ ions 262
4.2.5. SiF_x^+ ions 263
4.3. Synergistic effects 263
4.4. Surface composition and structure 265

5. Concluding remarks 268

Acknowledgements 268

References 268

Downloaded At: 15:50 21 January 2011

1. Introduction

Fluorocarbon plasma etching and plasma-enhanced chemical vapour deposition techniques are widely employed in scientific experiments and the microelectronic industries [1–8]. Plasma environments are inherently very complicated, consisting of ions, electrons and radicals. This complexity results in a wide variety of physical and chemical reactions that may occur at the surfaces with which they interact, as illustrated by Figure 1. As shown in the figure, a plasma will contain a mixture of neutral and charged particles, which may be inert or reactive. In addition, the surface itself may be composed of a variety of materials that will have different susceptibilities to modification via the plasma interaction. Neutral plasma species have a kinetic energy largely determined by the plasma temperature, and hence will only be of interest if they are capable of direct reaction with or at the surface. In contrast, the presence of a plasma-generated sheath potential in front of the surface means that ions can experience acceleration toward the surface. Consequently, ions with kinetic energies of tens or hundreds of eV may impact the surface and hence even 'inert' ionic species can play a significant role in plasma-induced surface modification.

It is both extremely difficult and time-consuming to develop a detailed understanding of plasma interactions at surfaces based solely on experimental investigations. Ideally, all the processes involved should be studied *in situ* and in *real time*. However, the complex coupling between plasma and surface makes it experimentally difficult to characterize reaction dynamics during the interaction. In order to fully understand such processes, a fundamental knowledge of plasma–surface interactions (PSIs) is needed. Establishing and quantitatively describing the mechanisms of plasma-induced surface reactions requires:

- characterization of the incident species fluxes, e.g. as a function of composition, energy, angle and internal state;

Downloaded At: 15:50 21 January 2011

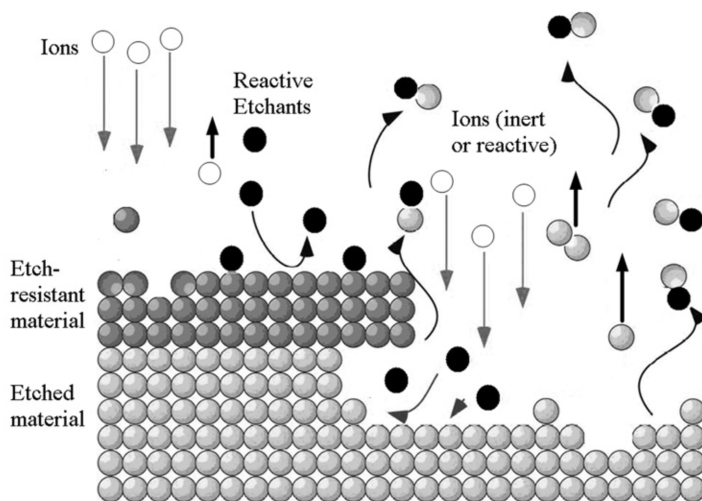

Figure 1. Schematic picture of plasma–surface interaction.

- determination of the surface processes (adsorption, reflection, direct and indirect reaction behaviour of the species, the surface coverage and the composition of the reaction layer);
- characterization of the reaction products ejected from the surface (their chemical identity, energy content, desorption mechanism, angular distribution, etc.).

Ideally we would like to characterize and quantify each of the elementary surface processes for important plasma and surface species, and relate these to measured etching or deposition rates and film properties.

1.1. *Experimental approaches*

The complexity of plasmas and the range of events that can occur at surfaces can make unambiguous interpretation of experimental data very difficult. In addition, the plasma represents a 'hostile' environment that limits the range of techniques that are available for *in situ* investigation. For analysis of the incident flux and the ejected reaction products, there are several techniques that are applicable for *in situ* measurement. Laser-induced fluorescence [9,10], line-of-sight plasma sampling by mass spectrometry [11], Fourier transform infrared (IR) spectroscopy or IR diode laser absorption spectroscopy [12] and UV absorption spectroscopy have all been employed [13–25]. Using these techniques, the incident flux can be relatively precisely characterized.

Downloaded At: 15:50 21 January 2011

Many powerful surface science tools, such as X-ray photoelectron spectroscopy (XPS) [26], Auger electron spectroscopy (AES) [27] and scanning electron microscopy (SEM) [28,29], are used for post-exposure characterization of surfaces. However, these measurements are generally performed under (ultra)-high vacuum conditions. Therefore the treated sample must usually be transferred from the reaction chamber to a suitable analysis chamber. As such, some assumptions need to be made when performing analyses on such surfaces. For example, transferring from a low vacuum to a high vacuum chamber should not change the surface composition or its properties. In most cases it is reasonable to make such assumptions, but caution should always be exercised. However, the most serious limitation remains the difficulty involved in reconstructing the plasma processes on the basis of post-exposure analysis. As a consequence, researchers turn to modelling and simulation techniques as a means to provide insight into the processes leading to the observed outcome. This manuscript deals with the applications of molecular dynamics (MD) simulations to problems applicable to plasma–surface interaction (PSI). Specifically, we restrict ourselves primarily to the interaction of fluorocarbons with silicon-containing surface.

1.2. *Theoretical approaches*

Many theoretical studies have been performed to better understand plasma mechanisms. In order to develop an understanding of plasma etching at the atomic level, MD simulations have been extensively used in recent years [30–42]. Such studies seek to elucidate the microscopic processes of plasmas interacting with surfaces. As with all modelling techniques, there is a trade-off between the level of detail that can be included in the model and the computation times required to achieve

usable results. For the MD method, this trade-off can be characterized by the choice between an *ab initio* and a classical description of the atoms in the system. Both approaches will be briefly introduced below with some references to relevant work. In practice, given the complexity of the systems and the number of atoms required to obtain reliable results, classical MD is currently the most realistic option for studying PSI-related systems.

1.2.1. Ab initio *molecular dynamics*

Ab initio molecular dynamics is a precise atomic simulation method that combines a quantum mechanical description of electronic structure with a classical description of atomic nuclei. This method has become a very powerful and valuable tool for the investigation of many physical and chemical processes [43–48]. It gives a more accurate description of the system than classical MD since it allows electronic behaviour to be considered. Hence, chemical reactions can be accurately described. Even reaction dynamics involving electronic transitions can be treated by utilizing specific dynamical techniques.

In etching involving F-containing plasmas, the interaction of F atoms with the surface plays a very important role since they are generally the most reactive species present. Thus, in the last decades, many density functional theory (DFT) based calculations have been utilized to study the processes relevant to F-related etching. In order to investigate the initial adsorption of F atoms on a Si(100) surface, Ezaki and Ohno performed first principles calculations [49]. Their simulation results show that at low F coverages the exothermal F–Si reaction resulted in the breaking of Si–Si bonds and thus a disordered Si surface was generated. At high F coverage, SiF_3 defects were produced on the surface. This phenomenon has been observed experimentally by Engstrom *et al.* [50]. They found a transition from the ordered Si(100)-2×1 surface to a disordered fluorinated Si surface during the initial exposure to F atoms. With increasing F exposure, XPS results showed that a new surface containing SiF, SiF_2 and SiF_3 species was formed. On the basis of this progression, it becomes reasonable to envisage that SiF_4 molecules will be ejected from the Si substrate as an etching product.

Downloaded At: 15:50 21 January 2011

Sasata *et al.* developed an accelerated quantum chemical molecular dynamics program based on the tight-binding theory [51]. They used the program to investigate CF_2 interacting with a SiO_2 surface. Their simulation results demonstrate that when energetic CF_2 bombards the surface, Si–O bond breakage and the formation of C–O and Si–F bonds occurs. These results are in good agreement with experimental data [52]. Kohler and Frauenheim employed a DFT based tight-binding method to simulate the interaction of CF_x ($x = 2$–3) radicals with amorphous and crystalline Si_3N_4 and SiO_2 surfaces [53]. In these simulations, binding and reaction energies were calculated and compared for different configurations. Their results indicate that the surface configuration (amorphous or crystalline) and the surface temperature will affect surface reactions.

However, the primary drawback of *ab initio*-based simulations is that they are a computationally intensive approach, which often requires the use of supercomputers. Although there has been some success in applying these methods to large systems, they are still too slow for the investigation of many interesting problems. This is particularly true of PSI investigations. Plasma-induced etching and surface modification generally occur on

a large scale and require a correspondingly large number of atoms in order to obtain a reliable simulation. Such systems are still beyond the practical scope of *ab initio* methods. Hence, for the remainder of this manuscript, we restrict our discussion to classical molecular dynamics simulations.

1.2.2. *Classical molecular dynamics*

Classical MD is an atomic simulation method for studying equilibrium and transport properties of large many-body systems. Relative to the time-consuming *ab initio* method, it is much less computationally intensive since the interactions between atoms are determined by predefined potentials in which no detailed description of electronic processes is included. The basic idea is to set up the system (initial velocities and positions) and to solve Newton's equations of motion for a collection of mutually interacting particles. The position and velocity can be solved by finite difference methods using a time interval that must be sufficiently small to conserve the total energy. The dynamics of the system are obtained by tracking trajectories of the individual atoms considered. Therefore, time-dependent properties of the system, such as scattering, implantation, sputtering of surface atoms and thin film growth are obtained.

Many classical MD simulations, based on a variety of empirical interatomic potentials that were developed from DFT calculations, have been performed over the last decades. A great deal of work has been performed for particle interaction with surfaces (at normal and grazing incidence), cluster beam deposition, annealing processes, the structure of thin films and the mechanical properties of multi-layer films. In addition, deposition and etching modelling, related to plasma–surface interactions, have been done using MD methods [30,32,35,37,54–69].

For Si–C–F systems, relevant covalent materials (such as single crystalline silicon, amorphous silicon, diamond and amorphous carbon), where (ideally) each atom has four nearest-neighbours in a tetrahedral arrangement, cannot be correctly described by a simple two-body potential. Due to this and other shortcomings, potentials incorporating many-atom effects have been developed in order to provide a more realistic description of such systems. One such empirical potential, initially constructed by Stillinger and Weber (SW) [70,71], includes two- and three-body interaction terms. Other models take into account the local environment (bond strength, length, type and angle) and allow the bond strengths to vary accordingly, such as the set of potentials developed by Tersoff [72–76]. In these potentials, the attractive term depends on the local environment of a specific atomic pair, which effectively includes many-body interactions. Brenner further developed this type of potential to describe systems containing hydrocarbons [36,77]. Garrison reviewed these potentials and their applications to surface reactions [78]. Abrams and Graves further extended the Tersoff–Brenner potential to encompass a C–F–Si system [30,34,79,80], while Humbird and Graves reparameterized the Si–F potentials using DFT [81]. Many simulations on the Si–C–F system have been performed using these potentials. In this paper, we will review some of the work done on modelling of plasmas (consisting of Ar^+, F, CF_x, SiF_x) interacting with various silicon surfaces.

Downloaded At: 15:50 21 January 2011

2. Simulation methods

2.1. *Classical MD simulations using empirical potentials*

It is important to note that the purpose of an MD simulation is not to predict *precisely* what will happen to a system that is initially in a well-defined state. In fact, for almost all systems, the trajectory of the system through phase space is sensitively dependent on the initial conditions. This means that the trajectories of two systems that are initially very close to one another may diverge exponentially as time progresses. The aim of the simulation is to predict the average behaviour of the system in a statistical sense.

The core of a molecular dynamics simulation is the interatomic potential. In classical MD, the forces exerting on each atom in the system are derived from a potential energy function V that is dependent on the coordinates of all particles in the system:

$$F_i = -\nabla V(r_1, \ldots, r_N). \tag{1}$$

Proper modelling of a material requires development and refinement of the potential function $V(r_1, \ldots, r_{\mathrm{N}})$ for that material. In classical simulations the atoms interact through two- and/or many-body interaction potentials. The highly complex description of electron dynamics is excluded and effective pictures of the processes involved are adopted. In this approach the main features, such as the hard core of the particles and the internal degrees of freedom, are modelled by a set of parameters and analytical functions, which depend on the mutual positions of the atoms in the configuration. These parameters and functions give information about the system energy and the forces acting on each particle.

Due to its tremendous importance for diverse technological and industrial applications (e.g. etching), fluorine-based plasma interactions with silicon surfaces constitute a field of intense research, with a large range of applications and many fundamental issues. In order to aid interpretation of experimental data and to gain insight into the interaction mechanisms, many classical MD simulations have been conducted. Consequently many potentials, both general and system-specific, have been developed, with various degrees of success [33,82,83]. Of these potentials, the SW and Tersoff–Brenner potentials mentioned earlier are among the most widely used. Hence, we will continue by giving a brief outline of these two potentials.

Downloaded At: 15:50 21 January 2011

2.1.1. *SW potential*

The SW potential was one of the first attempts to model a semiconductor using a classical model. It is based on a two-body term and a three-body term [70,71,84]:

$$V = \varepsilon A\left[\sum_{(ij)} v_{ij}^{(2)}(r_{ij}) + \frac{\lambda}{A}\sum v_{jik}^{(3)}(r_{ij}, r_{ik})\right] \tag{2}$$

where the two-body part is given by

$$v_{ij}^{(2)}(r_{ij}) = \left[B\left(\frac{r_{ij}}{\sigma}\right)^{-p} - 1\right]\exp\left(\frac{1}{r_{ij}/\sigma - a}\right) \times \Theta\left(a - r_{ij}/\sigma\right) \tag{3}$$

and the three-body part is given by

$$v_{jik}^{(3)}(r_{ij}, r_{ik}) = \exp\left[\frac{\gamma}{r_{ij}/\sigma - a} + \frac{\gamma}{r_{ik}/\sigma - a}\right]\left(\cos\theta_{jik} - \cos\theta^{\circ}\right)^2 \Theta\left(a - \frac{r_{ij}}{\sigma}\right)\Theta\left(a - \frac{r_{ik}}{\sigma}\right) \quad (4)$$

Here, $\Theta(x)$ is the Heaviside step function and θ° is the desired interbond angle. In the case of Si, this is the tetrahedral angle ($\cos\theta^{\circ} = -1/3$). Consequently bond angles are as close as possible to those found in the diamond-like tetrahedral structure and this is the most stable structure for this potential.

Due to its relative simplicity and inherent physical description of crystals with a diamond-like structure, a number of simulations have been performed for Si systems by means of the SW potential [70,71,84–88]. Schoolcraft *et al.* performed MD simulations to study the adsorption of fluorine molecules on a clean Si(100)-2×1 surface at 1000 K [60]. Weakliem and coworkers adjusted the F–Si interaction potential by fitting the functions of the SW potential to first-principles quantum mechanical calculations [89,90]. Based on their improved SW potential, they reported that an initial build-up of a fluorosilyl layer was necessary for subsequent etching. Numerous simulation results show that these improvements to the SW potential provide a better description of reactions occurring on surfaces [89,90]. However, the built-in tetrahedral bias of the SW potential results in problems of transferability to non-crystalline systems. For instance, SW cannot properly predict the correct energies of the non-tetrahedral structures found under certain circumstances.

Downloaded At: 15:50 21 January 2011

2.1.2. *Tersoff–Brenner potential*

The other widely used potential, initially developed by Tersoff, is based on the concept of bond order and includes an angular contribution to the forces [72–76]. In this type of potential, the strength of a bond between two atoms is not constant, but varies depending on the local environment. The inclusion of bond order means that the TB potential is extremely useful for predicting bond breaking and bond formation. Many groups have further developed the original potential in order to expand the range of systems that can be studied. The potential is widely used at present in various applications for silicon, carbon and germanium. Based on DFT calculations and experimental data, Graves and coworkers further developed the TB potential to describe the C–F–Si system potentials [31, 33]. The system potentials have the form:

$$E_b = V_R(r_{ij}) - \bar{b}_{ij} V_A(r_{ij}) \quad (5)$$

where E_b is the binding energy and r_{ij} is the distance between atoms i and j. $\bar{b}_{ij}$ is a many-body empirical bond-order term (detailed below). V_R is used to describe the interatomic core–core repulsive interactions, and V_A is to model the attractive interactions due to the valence electrons. These terms have the following forms:

$$V_R(r_{ij}) = f_{ij}(r_{ij}) A_{ij} \exp(-\lambda_{ij} r_{ij}) \quad (6)$$

and

$$V_A(r_{ij}) = f_{ij}(r_{ij}) B_{ij} \exp(-\mu_{ij} r_{ij}) \quad (7)$$

where A_{ij}, B_{ij}, λ_{ij} and μ_{ij} are fitting parameters and f_{ij} is a smooth cutoff function given by:

$$f_{ij}(r_{ij})=\begin{cases} 1 & \text{if } r_{ij}<R_{ij}^{(1)} \\ \frac{1}{2}-\frac{9}{16}\sin\left(\pi\frac{r_{ij}-\left(R_{ij}^{(2)}+R_{ij}^{(1)}\right)/2}{R_{ij}^{(2)}-R_{ij}^{(1)}}\right)\left(-\frac{1}{16}\sin 3\pi\frac{r_{ij}-\left(R_{ij}^{(2)}+R_{ij}^{(1)}\right)/2}{R_{ij}^{(2)}-R_{ij}^{(1)}}\right) & \text{if } R_{ij}^{(1)}<r_{ij}<R_{ij}^{(2)} \\ 0 & \text{if } r_{ij}>R_{ij}^{(2)} \end{cases} \quad (8)$$

The use of sinusoidal functions leads to a continuous variation of the value of this function from 0 to 1 within the range of R_{ij} resulting in a smoother potential. The use of a cutoff function minimizes the computational expense while maintaining a good energy and momentum conservation (<0.2%), since at any given time the number of atom pairs within the cutoff region is small compared to the entire system.

The bonding between atoms is determined by the local environment through the many-body empirical bond-order term, $\bar{b}_{ij}$. It modulates the valence electron densities and depends on atomic coordination and the bond angles. It has the form:

$$\bar{b}_{ij}=\frac{1}{2}\left[b_{ij}+b_{ji}+F_{CC}\left(N_{ij}^{(t)},N_{ji}^{(t)},N_{ij}^{(\mathrm{conj})}\right)\right] \quad (9)$$

where F_{CC} is the Brenner-type correction function for a C–C bond. b_{ij} is the contribution of atoms adjacent to atom i to the bond order of the ij bond:

$$b_{ij}=\left\{1+\left[\zeta_{ij}+H_{ij}\left(N_{ij}^{(F)},N_{ij}^{(C)}+N_{ij}^{(Si)}\right)\right]^{\eta_i}\right\}^{-\delta_i}. \quad (10)$$

Figure 2 shows the potential energy as a function of the distance between Si and F atoms for three different bond order values. As seen in Equation (5), $\bar{b}_{ij}$ is a multiplier of the attractive part of the potential. Hence, with decreasing $\bar{b}_{ij}$, a transition from a partially attractive potential to a purely repulsive potential occurs.

In Equation (10), H_{ij} is the correction function. $N_{ij}^{(\mathrm{F})}$ and $N_{ij}^{(\mathrm{Si})}$ are coordination numbers. ζ_{ij} is a bond competition function, modelling the bond lengths and bond angles:

$$\zeta_{ij}=\sum_{k\neq j}f_{ik}(r_{ik})g_i(\theta_{ijk})\exp\left\{\alpha_i\left[\left(r_{ij}-R_{ij}^{(e)}\right)-\left(r_{ij}-R_{ik}^{(e)}\right)\right]^{\beta_i}\right\} \quad (11)$$

$R_{ij}^{(e)}$ and $R_{ik}^{(e)}$ are the equilibrium dimer bond lengths between atoms i and j and between atoms i and k, respectively. θ_{ijk} is the angle between the bonds ij and ik. $g_i(\theta_{ijk})$ is the potential energy penalty of changing a bond angle:

$$g_i(\theta_{ijk})=a\left(1+\frac{c^2}{d^2}-\frac{c^2}{d^2+(h-\cos\theta)^2}\right) \quad \text{if } i\in \mathrm{C} \quad (12)$$

and

$$g_{Si,F}(\theta)=c+d[h-\cos\theta]^2 \quad \text{if } i\in \mathrm{Si,F}. \quad (13)$$

The potential parameters are chosen by fitting experimental data and theoretical results obtained for realistic and hypothetical silicon configurations.

Downloaded At: 15:50 21 January 2011

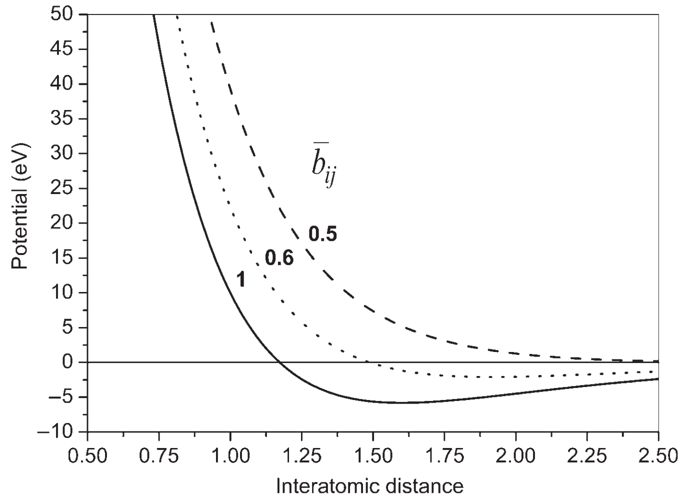

Figure 2. The potential energy as function of the distance between Si and F atoms for $\bar{b}_{ij} = 1.0$, 0.6 and 0.5.

Downloaded At: 15:50 21 January 2011

2.1.3. *Improving the potentials*

Abrams and Graves made a comparison for reactive F^+ ion etching of Si between the SW and Tersoff (T) potentials used within their group [34]. Figure 3 shows the potential energy between molecular SiF (bond length of 1.6 Å) and a free F atom as a function of the F–F distance for the SW and T potentials used. In the SW potential, a description of physisorption was included, corresponding to the small (0.05 eV) local minimum at about 3.4 Å. In the T potential, when the F atom is beyond the cut-off range ($R_{\text{cnt}} = 2$ Å), no interaction occurs. As the free F approaches the SiF molecule, the repulsive potential between SiF and F shows a sharp increase. The different potentials produced different Si etch rates, surface structure and composition and etching mechanisms. It was found that almost no chemical sputtering occurred for the Tersoff-form potential, while for the SW potential chemical sputtering was dominant for incident energies from 10 to 50 eV. The difference was attributed to the shorter range of interactions in the T potential and the fact that a physisorption well was constructed in the SW potential but was absent from the T potential. As a result, clusters desorbing in the SW simulation could experience a weak attraction to the surface and hence be counted as 'chemically-sputtered'. No such interaction could occur for the T-potential and such clusters would be counted as 'physically-sputtered'.

With increases in computing power and the desire to understand dynamics occurring at surfaces during etching on the atomic level, many researchers have made quantitative improvement in the accuracy of the two potentials outlined above. Carter and coworkers improved the SW Si–F potential based on *ab initio* calculations [91]. Using this type of improved potential, Barone and Graves performed MD simulations to investigate chemical and physical sputtering of fluorinated silicon [35]. Figure 4 show the resulting physical- and chemical-sputtering yields obtained for 200 eV Ar bombardment as a function of the F/Si ratio in the substrate. At low ratios (F/Si $<$ 0.5) physical sputtering

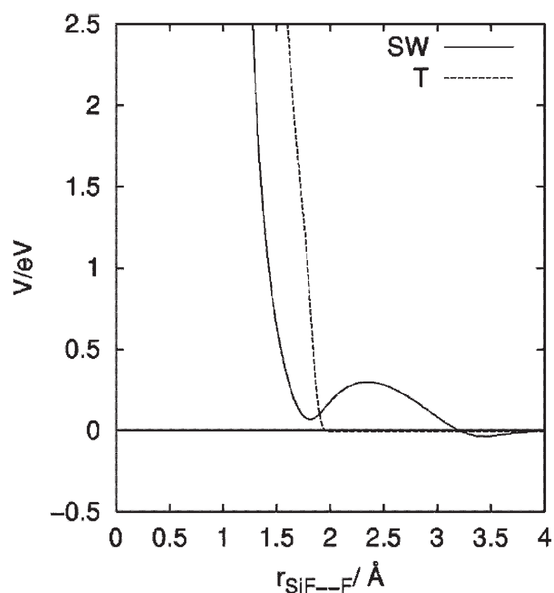

Figure 3. Potential energy of the Si–F–F triplet (reference to an Si–F dimer and F atom at infinite separation) as a function of F–F separation distance with the Si–F distance fixed at 1.6 Å for the Stillinger–Weber (SW) and Tersoff-form (T) potentials. (Reused with permission from Cameron F. Abrams, Journal of Applied Physics, **88**, 3734 (2000). Copyright 2000, American Institute of Physics.)

Downloaded At: 15:50 21 January 2011

was dominant, while at higher levels of fluorine incorporation in the silicon layer ($F/Si > 0.8$) chemical sputtering becomes dominant. Abrams and Graves performed simulations of CF_x ions interacting with silicon surfaces [30,31,33]. In the initial Si–C–F system potential, the three-body parameters of the Si–F potential were simply taken as those of Si–H. Humbird and Graves produced improved empirical interatomic potentials for Si–F and Si–Cl based on DFT cluster calculations [81]. Their potential allowed simulation of spontaneous etching of Si by F [39].

2.2. *Sample preparation*

In order to perform MD simulations, suitable initial model surfaces must be created. The precise details of sample preparation and particle interaction may vary from group to group, although the broad outline will be the same. For the purposes of this text, we will present the details regarding the specific approach used in our group. Generally, a simulation cell is established with periodic boundary conditions in the x- and y-directions, while the bottom layers are fixed in order to maintain the structure. The bulk of atoms in the cell are movable under force. The dimensions of the cell are largely determined by the competing requirements of producing an accurate simulation with no artifacts generated by the constraints (sufficiently large) while remaining computationally realistic (no larger than necessary). The two most critical factors influencing the cell size are the incident energy and the incidence angle

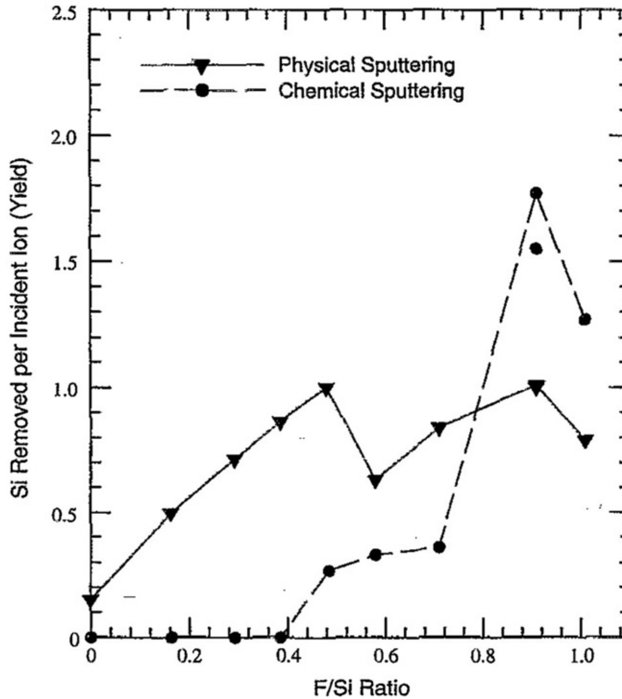

Figure 4. Physical and chemical Si sputtering yields for fluorinated Si bombarded by 200 eV Ar. (Reused with permission from M.E. Barone, Journal of Applied Physics, **77**, 1263 (1995). Copyright 1995, American Institute of Physics.)

Downloaded At: 15:50 21 January 2011

of the plasma particles. Higher incident energies require larger simulation cells (in all three coordinates). Off-normal incidence angles may require expansion of the cell in the x- and/or y-directions. In some instances this can be partially compensated for by a reduction in the z-dimension of the cell.

In order to simulate the etching process, particles are impinged on the surface. Typically, particles are treated in a sequential fashion. Hence, concerted effects that might occur under high flux conditions are outside the scope of the material presented in this manuscript. At the beginning of each trajectory, the incident particle (atomic or molecular) is placed at a randomly chosen location above the target. In the case of molecules, the initial orientation is also randomly selected. The incident energy and incidence angle are preselected quantities. Depending on the objective of the simulation, these may be fixed quantities or randomly selected from a required parameter range. The trajectory of each incident particle is integrated individually and, after each integration is completed, atoms and molecules that are deemed to be not bonded to the surface are removed from the configuration before a new particle is directed at the surface. Typically the simulation of each particle is run for a preset finite time. As with the determination of the appropriate cell size, the trajectory time should be sufficiently long to accurately reflect the interaction dynamics while remaining computationally realistic.

Downloaded At: 15:50 21 January 2011

It is important that the results of a simulation be presented in an experimentally-relevant fashion. One suitable method is to plot simulated results as a function of exposure, typically expressed in units of monolayer (ML). The total ML exposure is obtained by dividing the total number of molecules that have struck the surface by the number of atoms in the outermost layer of the original (ideal) surface. The adsorbed coverage, based on the number of a particular species that stick to the surface, and the etch yield can also be expressed in units of ML. Frequently there will be a significant disparity between results obtained during the early stages of a simulation (during exposure of a clean, unperturbed surface) and those obtained once a steady-state condition has been established. Physical quantities determined after the steady-state has been established are generally the most relevant for comparison to experiment data. In the current work, in addition to referencing already published results, some new simulations of CF_3 interaction with Si are presented. In addition to the details provided for those specific calculations, the reader is referred to the simulations conditions as outlined in previous publications [61–64, 92] for further details regarding the simulation method.

In MD simulations, many factors, such as incident energies, incidence angles, incident species and surface temperature, may affect the final results. In addition, many simulation-related factors such as the parameters within the potential, the integration method, the cell size, the heat bath (i.e. the energy balance mechanism) and the time-step, may alter the microscopic dynamics and ultimately influence the results. Some factors will only slightly affect the results, while others may significantly alter the final outcome. We will continue by illustrating the effects of some important factors on the simulation. This will serve both to introduce the simulation method and to provide an indication of the reliability of the generated results.

2.3. *Effects of the simulation method*

The methods and parameters employed during an MD simulation can have a significant effect on the results of the calculation. It is always essential to check that the methods and approximations used are valid and reasonable. In order to illustrate the effect of various critical parameters on the outcome of etching simulations, we will provide some selected examples based on CF_3 ions interacting with a Si(100)-2 $\times$ 1 surface. In all cases the CF_3 molecules are incident along the normal direction with an energy of 100 eV. The orientation of the molecule with respect to the surface is chosen randomly.

2.3.1. *Temperature control mechanism*

When an energetic molecule collides with a surface some of its translational energy is lost. The magnitude of the energy loss depends on the incident energy and the effective masses involved in the impact. In scattering calculations, most of the translational energy lost is transferred to surface atoms (the remainder goes to dissociation of, or internal energy uptake by, the molecule) [37]. The energy gained by the sample in this manner cannot escape naturally from the 'substrate' because periodic boundary conditions are typically adopted. In a real system, the energy deposited in a small region near the surface is dissipated by phonon propagation leading to thermal conduction. Since periodic boundaries prevent the heat from dissipating out of the system, dedicated

cooling processes are necessary to prevent unrealistically over-heating. In order to remove the energy added to the cell from the simulation, various schemes have been developed. Examples include the Andersen thermostat [93], the Nosé–Hoover thermostat [94] and the Berendsen thermostat [95]. All three are briefly outlined below. The roles of these three thermostats in simulations have been investigated by Erhart and Albe [96]. The different methods utilize an external heat bath to control the sample temperature. They differ in the precise means by which the heat bath and the simulated system are coupled to each other. For all simulation performed by our group the Berendsen thermostat has been used.

2.3.1.1. *Nosé–Hoover thermostat*. This extended Lagrangian method was initially introduced by Nosé [94,97,98] and subsequently developed by Hoover [99,100]. This method uses the external heat reservoir to add additional degrees of freedom to the system, controlling the temperature via the exchange of kinetic energy. The interaction between the heat reservoir and the simulated system maintains the desired temperature, which fluctuates around the preset value. The Lagrangian equations can be written as:

$$\ddot{r}_i = \frac{F_i}{m} - \xi \dot{r} \tag{14}$$

where F_i is the force exerting on atom i. The thermal dynamic friction ξ is integrated according to

$$\dot{\xi} = \left(\frac{T - T_e}{T_e}\right)\frac{1}{\tau^2}. \tag{15}$$

This method can precisely reproduce the canonical ensemble.

Downloaded At: 15:50 21 January 2011

2.3.1.2. *Andersen thermostat*. In the method proposed by Andersen, the temperature is controlled via the collision of particles, randomly selected from the simulated system, with the heat bath [93]. The effect of the collision is to change the momentum of the colliding particle(s) to a value drawn from the system at the desired temperature. Assuming successive collisions are uncorrelated, the distribution of time intervals between successive collisions satisfies the Poisson form

$$p(v, t) = v\ \exp(-v \cdot t). \tag{16}$$

The collision probability during a time-step of length Δt is given by $v\Delta t$. v denotes the collision frequency. If the selected particle undergoes a collision, its new velocity will be obtained from a Maxwell–Boltzmann distribution corresponding to the preset temperature. All other particles in the system are unaffected by this collision.

2.3.1.3. *Berendsen thermostat*. The Berendsen scheme is widely used in PSI simulations [32,101]. The heat bath acts to supply or remove heat to/from the system as appropriate. The basic mechanism is to rescale the velocities of the atoms in the system in order

to achieve a mean kinetic energy consistent with the target bath temperature at each time-step. The rescaling is done by a factor, λ:

$$\lambda = \left[1 + \frac{\delta t}{\tau_T}\left(\frac{T_{\text{set}}}{T} - 1\right)\right]^{1/2}. \tag{17}$$

Here, δt is the time-step, T_{set} is the set-point temperature, and T is the instantaneous temperature computed over the course of the simulation. τ_T is the rising time of the heat bath. A small τ_T corresponds to a stronger heat bath (faster response) relative to a large τ_T.

This algorithm is especially suitable for non-equilibrium molecular dynamics since local disturbances are kept to a minimum while preserving global gradients [102]. This method has been widely used in MD simulations of energetic particles interacting with surfaces.

2.3.2. *Thermostat parameters*

Quite apart from the precise approach adopted for temperature control, all of the schemes have variable parameters that dictate the responsiveness of the thermostat to deviations from the preset sample temperature. Modification of these parameters can allow for extremely slow or fast cooling if desired, or inadvertently through poor value selection. The effect of the thermostat on the simulation can be modified by both external (the time at which the heat bath is applied) and internal (the strength of coupling between the heat bath and the system) factors. The following section demonstrates the influence of these factors for the specific case of the Berendsen heat bath.

Downloaded At: 15:50 21 January 2011

2.3.2.1. *Application time.* During a simulation the heat bath can be applied either over the entire impact integration time or for only some latter portion of it. For this illustration, we tested three modes of applying the Berendsen heat bath for individual CF_3 molecules colliding with a Si(100)-(2 × 1) surface. The incident energy is 100 eV and the incidence direction is along the surface normal. Each trajectory is simulated for a total of 5 ps and the sample set-point temperature was 300 K. The first heat removal strategy is to apply the heat bath during the entire trajectory, referred to as MOD1. The second is to switch on the heat bath after each trajectory had run for 0.2 ps and the third is to switch on the heat bath after 0.4 ps, referred to as MOD2 and MOD3, respectively. All other simulation conditions were unchanged for the three modes.

Figure 5 shows the instantaneous temperature of the sample as a function of time for the three models. The sharp increase in the sample temperature, which occurs shortly after the start of each simulation, marks the main impact of the incident molecule with the surface. In all cases, application of the heat bath results in a rapid cooling of the sample back to its set-point temperature. In the case of MOD2 and MOD3 the point at which the heat bath is applied can be readily identified from the temperature plots. It is clear from the figure that a long delay between the initial impact and the application of the heat bath results in the sample 'equilibrating' at a higher temperature for a period of time.

The data shown in Figure 5 for the three modes are each for a single trajectory. In order to judge the effect of the different modes on the overall results, simulations for a total exposure of 20 ML were performed for all three. The uptakes of C and F atoms by

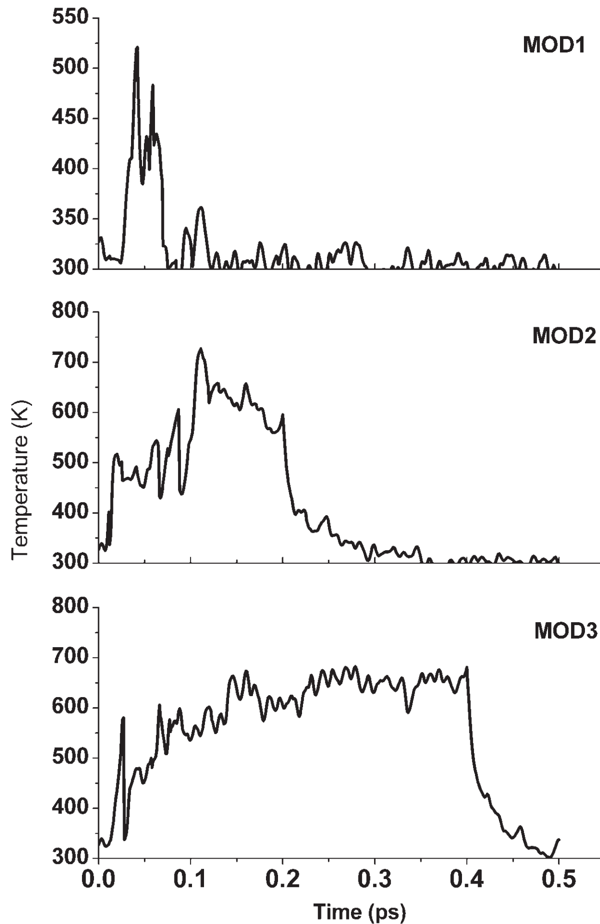

Figure 5. Instantaneous temperature of the sample as a function of time for three different heat bath application times. 100 eV CF_3 incident on Si(100)-2 × 1.

Downloaded At: 15:50 21 January 2011

the surface as a function of exposure were essentially identical for the different modes (data not shown). Hence, the heat bath application time had no significant effects on the surface coverages predicted. In contrast it did have a significant effect on the predicted etching rate. Figure 6 shows the Si etching yield determined as a function of exposure for the three modes. There is a difference between MOD1 and MOD2, while no significant difference is observed between MOD2 and MOD3. MOD1 gives the lowest predicted etch rate. Clearly, the period during which the substrate is at an artificially elevated temperature (prior to application of the heat bath) prompts additional weakly-bound species to leave the surface. The effect is not progressive; significantly extending the period of elevated temperature (going from MOD2 to MOD3) does not produce a correspondingly large change in the etch rate. Hence, the elevated temperature acts to remove weakly bound species that are present on the surface, but does not significantly influence the number of such species that exist.

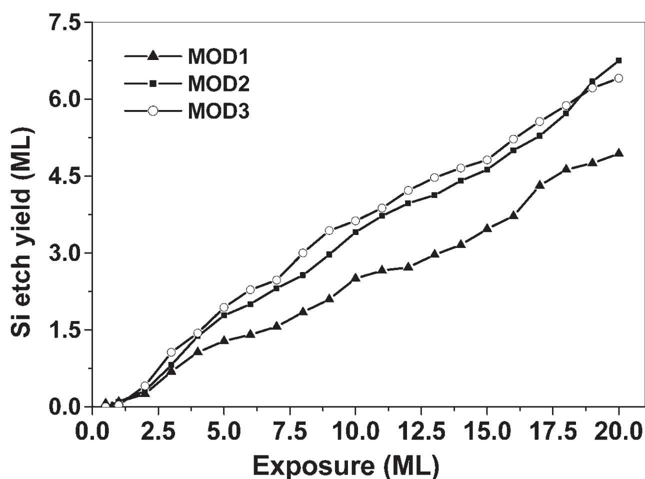

Figure 6. Si etching yield as a function of the exposure for 100 eV CF_3 incident on Si(100)-2 × 1 with the three different application times of the heat bath.

Downloaded At: 15:50 21 January 2011

Figure 7 shows the final atomic densities in the sample as a function depth for MOD1, MOD2 and MOD3 after the exposure to 20 ML CF_3. In all three cases a mixed Si/C/F reaction layer is formed on top of the bulk Si layers. From the figure we note that delaying the application of the heat bath results in the peaks of C and F being shifted more toward the bulk. This is a consequence of the higher etch rate of Si. Comparing MOD1 to MOD2 and disregarding the positional difference due to the etch rates, the atomic distributions in the reaction layer are reasonably similar in terms of shape and absolute density. However for MOD3, while the etch yield of Si atoms is similar to that of MOD2, the atomic distributions in the reaction layer are completely different. MOD3 produces the broadest distribution of F and C atoms and the density profile indicates the formation of a layered structure, with a C-rich outer layer covering a more F-rich deeper region. The long delay before application of the heat bath results in the sample temperature remaining unphysically high in MOD2 and MOD3. This appears to promote intermixing resulting in a (too-) broad reaction layer. Unlike Si etching, the distribution of atoms in the reaction layer is strongly influenced by the length of time that the sample is maintained at the elevated temperature. Hence, it is important to ensure that the heat bath is applied sufficiently early in the integration process to avoid unwanted annealing effects.

2.3.2.2. *Coupling strength*. For the Berendsen thermostat, the strength of the coupling between the reservoir and the system is determined by the rising time, τ_T. In simulations by Barone and Grave using the SW potential and the Berendsen scheme, the rising time was found to have relatively little effect on the overall etching yields, although it did alter the ratio of chemical versus physical sputtering determined [35]. They found that the physical sputtering yield was most sensitive to the heat removal scheme used. This was observed to be mainly due to a small number of rather high-yield (unphysical) events rather than a more general increase in the yield/impact. In our simulations we typically use a rising time of 0.01 ps, consistent with work of Abrams and Graves [30,33]. Figure 8(a) shows how the

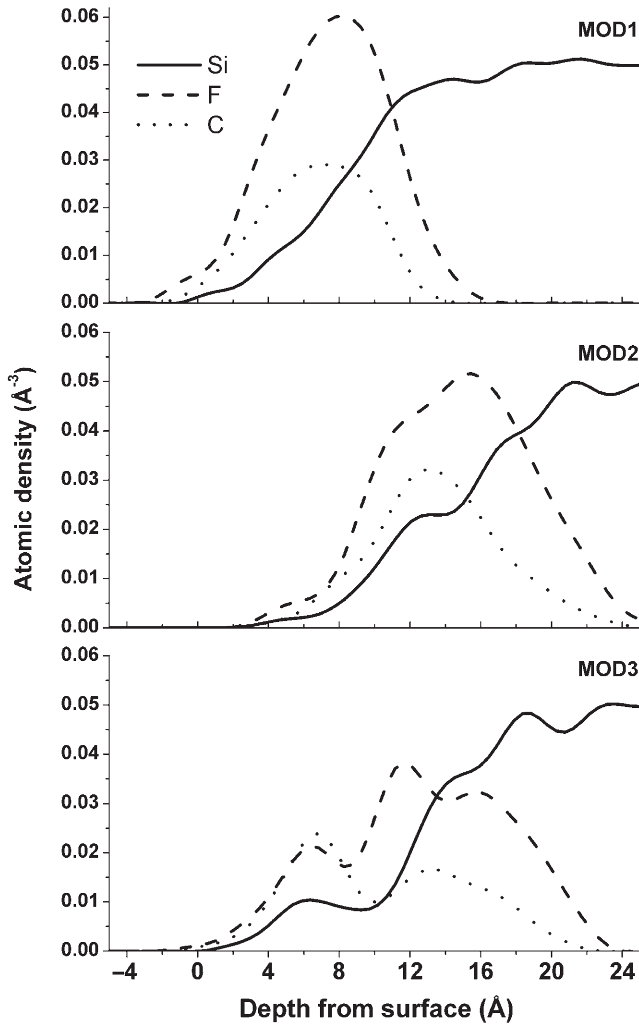

Figure 7. Atomic densities of the sample as a function of the depth for MOD1, MOD2 and MOD3 after exposure to 20 ML of 100 eV CF_3.

Downloaded At: 15:50 21 January 2011

scaling factor λ varies as a function of the rising time τ_T. This is based on an instantaneous temperature (T in Equation 18) of 600 K, a T_{set} of 300 K and δ_t of 0.001 ps. λ is less than 1 because T is larger than T_{set}; the further λ is from 1, the quicker the instantaneous temperature converges to T_{set}. From the figure, we note that λ gets smaller with shorter rising time illustrating that if τ_T is small, coupling (heat exchange) will be stronger. Figure 8(b) shows how the sample temperature responds to application of the heat bath with two different rising times. By making the rising time sufficiently small a near-instantaneous (on the simulation time-scale) change in temperature can be realized. However, simulation results (C and F uptake and Si etch rates; data not shown) did not show any significant differences between three different rising times (0.005, 0.01

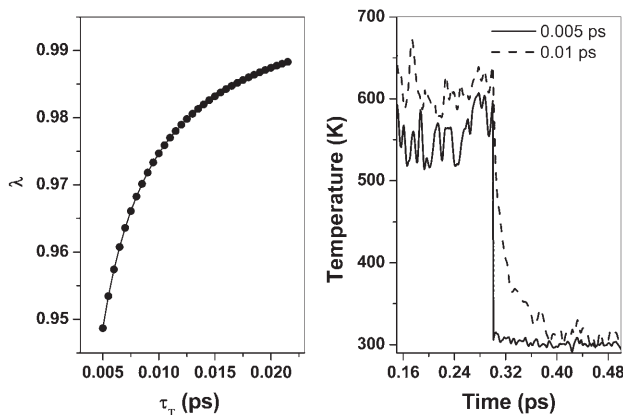

Figure 8. (a) Scaling factor λ variation as a function of the rising time τ_T. (b) Evolution of the Si sample temperature during impact by a single 100 eV CF_3 for rising times of 0.005 and 0.01 ps.

and 0.05 ps), indicating that the results (in this particular case) are not particularly sensitive to the rising time applied.

Downloaded At: 15:50 21 January 2011

2.3.3. *Simulation time-scale*

As discussed previously, bombardment of the sample cell is simulated by individual molecules incident in a sequential fashion. The trajectories of the incident molecules are calculated in discrete time-steps. It is necessary to establish that the size of the time-step used and the total integration time permitted per individual trajectory do not unrealistically influence the simulated result. Changes may arise if the sample does not have time to fully equilibrate during the integration time of a single trajectory. Related to this, it should also be established if allowing a period of post-bombardment relaxation of the sample cell has an effect on the final results.

2.3.3.1. *Time-step.* In MD simulations the positions and velocities of atoms are obtained by integrating Newton's equations of motion. In our group, the velocity–Verlet scheme has been used to perform this integration [37,55,92]. This scheme computes the particle velocity $v(t+\mathrm{d}t)$ and position $x(t+\mathrm{d}t)$ at time $t+\mathrm{d}t$ as follows:

$$x(t+\mathrm{d}t) = x(t) + v(t)\mathrm{d}t + \frac{1}{2}\mathrm{d}t^2\frac{f(t)}{m} \tag{18}$$

$$v(t+\mathrm{d}t) = v(t) + \frac{f(t)+f(t+\mathrm{d}t)}{2m}\mathrm{d}t \tag{19}$$

where $\mathrm{d}t$ is the time-step, m is the particle mass and $f(t)$ is the total force acting on the particle at time t. Given the initial conditions $x(0)$ and $v(0)$, one can compute $v(t)$ and $x(t)$ simply by applying these two equations successively n times, with $n = t/\mathrm{d}t$.

The selection of the time-step is the most critical aspect of the integration process. As before, we ran simulations of 100 eV CF_3 bombarding Si(100) in order to test the

influence of the time-step on the uptake of C and F and on Si etching. For these simulations, values of dt ranging from 0.5 to greater than 1 fs were tested. Two criteria can be used to judge the suitability of a given time-step. The first is the total energy of the system. Over the course of a trajectory calculation this should not change significantly. In our simulations, typically we seek to ensure a total energy drift during the collision of less than 0.1%. In our test simulations, time-steps greater than 1 fs could not be used if such a criterion is to be adhered to. Such an upper-limit will exist for any incremental integration scheme. It is crucial that the selected time-step be sufficiently small to prevent the total-energy deviation exceeding a predetermined limit. The second criterion that can be used to judge the adequacy of the time-step is comparison of the final results. For the test calculations performed time-steps ranging from 0.5–1 fs had little effect on the surface coverage of C and F or on the etching of Si (data not shown). A shorter time-step for a fixed overall integration time means a longer computation time. Provided the overall energy of the system does not change significantly, the longest time-step (1 fs in this case) should be chosen in order to minimize the overall computation time.

Downloaded At: 15:50 21 January 2011

2.3.3.2. *Integration time*. Over the course of the integration period of a single trajectory, the incident CF_3 may be adsorbed on the surface, scattered away, or (in the case of collision-induced dissociation) some combination of sticking and scattering may occur. Removal of surface atoms may occur either by immediate sputtering or by chemical reaction to form molecules that are not strongly bound to the substrate. The total integration time of a single impact must be at least long enough to allow an incident molecule to complete its interaction (deposition of energy) with the surface. Once this criterion is satisfied, a longer integration time means, in effect, relaxation of the substrate for a longer interval between impacts (as opposed to the final relaxation period outlined below). Test simulations done for integration times ranging from 0.25 to 1.0 ps did not show sensitivity to the integration time (data not shown). A significant difference should only occur if the integration time used is too short. Note that the integration time is significantly influenced by the velocity and angle of incidence of the impinging particle. More grazing angles and slower molecules require longer integration times.

2.3.3.3. *Relaxation time*. Somewhat related to the integration time is the possibility that allowing a post-bombardment relaxation of the simulated system may result in quantifiable changes. Allowing an extended period of post-bombardment relaxation may result in an equilibration that is not permitted to occur under the more dynamic conditions of 'continuous bombardment'. Using the test system of 100 eV CF_3 bombarding Si(100), the atomic composition and distribution of an 'unrelaxed' surface (the surface immediately after the final trajectory has finished) was compared to the same system after an additional 20 ps relaxation period. No significant differences between the two surfaces were found (data not shown). In addition, during this period no particles were found to desorb from the surface, hence the overall composition did not change and we can consider modified surfaces in this system as stable immediately after completion of etching.

2.3.4. *Cell size effect*

In the last decade with significant improvement in computational power, larger and larger simulation cells have become viable. However, limitations of simulation cell size still remain a practical reality and it is generally desirable to keep the simulation cell as small as is permissible. It is important to establish that the initial size of the simulated cell does not unduly influence the final results. The development of defect structures is one particular example of features that can be critically affected by the cell size. Surfaces are damaged as a result of bombardment by energetic species and vacancies and holes may be formed as a result. This surface roughening is critical since, during the etching processes, it allows incident species to deposit energy and atoms deeper in the sample. For the specific case of CF_3 bombarding Si, more F atoms can be transported into the substrate and may react with Si to form weakly bound SiF_x species. These species can desorb from the sample via the same vacancies through which the incident molecules entered. In MD simulations the application of periodic boundaries inherently prohibits the formation of roughness on length-scales larger than the cell size. With increasing cell size, the length-scale of the surface roughness that can develop increases and this may play a role in enhancing the etching. As an illustration, comparison is made of etching of three different Si(100) cell sizes by 100 eV CF_3. As for the previous examples the incidence direction was normal to the surface. In this instance the initial cell configurations were for single crystal samples consisting of $3 \times 3 \times 4$, $4 \times 4 \times 6$ and $5 \times 5 \times 10$ Si (100) unit cells. The respective cells consisted of 288, 768 and 2000 Si atoms with surface areas of ~200, ~500 and ~730 Å^2. The corresponding surface layers containing 18, 32 and 50 atoms and the samples had depths of ~20, ~35 and ~55 Å, respectively. The total exposure to CF_3 was equivalent to 20 ML.

Figure 9 shows the comparison of the simulation results for C and F uptake and for Si etching. At the end of the simulation all three cell sizes exhibit roughly equivalent coverages of C and F – indicating that the uptake probabilities are relatively independent of the sample size. Note however that over the course of the exposure the coverages of C do not always correlate well. In contrast, the uptake of F is essentially identical for all three samples over the course of the simulation. In the case of carbon, the smallest cell size is the quickest to reach the final 'equilibrium' C coverage. As the cell size increases the C-coverage tends to initially overshoot before returning to a stable level. The corresponding Si etch rate plots show that the predicted rate increases as the sample size increases. The behaviour of both the C uptake and Si etching is due to the ability to generate different length-scale roughness on the surface. In the case of C uptake, the upper limit on the coverage is provided by the growth of a SiC surface layer that reaches a 'saturation' level. The simulation is effectively tracking the progression of the surface from a well-ordered Si(100)-2×1 structure to a disordered SiFC reaction layer. Increased surface roughness (hence surface area) during the course of this transition allows the C coverage on the larger samples to exceed the final equilibrium value. However, progressive etching and the emergence of a steady-state reaction layer ultimately drives all values back to the equilibrium level. Equally, an increased effective surface area leads to a higher observed etch rate. Note however that the different etch rates persist to the end of the current simulation. In the first instance this reflects the continuation of Si etching even in the presence of a CF layer. In addition, the higher rates are attributable to a more open and porous reaction-layer structure being formed on the larger cell size. This permits a

Downloaded At: 15:50 21 January 2011

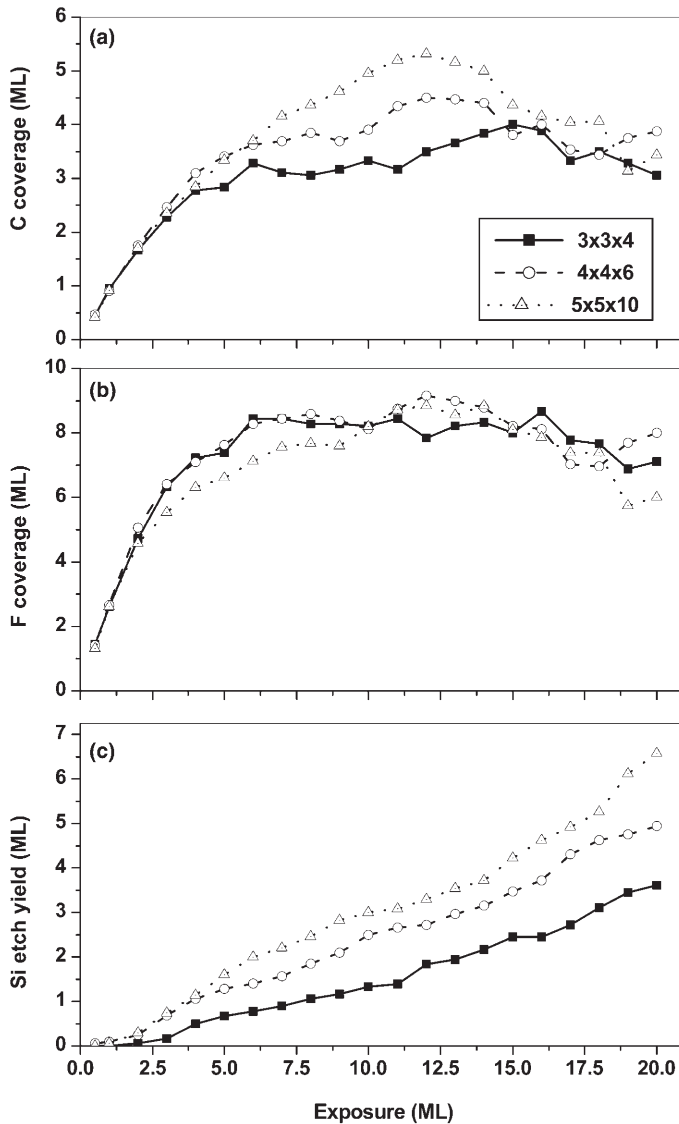

Figure 9. Coverages of (a) C and (b) F atoms on the sample as a function of exposure to 100 eV CF_3 for the three Si sample sizes; (c) Si etching yield as a function of the exposure.

Downloaded At: 15:50 21 January 2011

higher etch rate [58]. It is clear from the results that, if the cell size adopted is too small, unwanted structural effects (in this case the inability to create a sufficiently ‘open’ structure) can influence the results. Great care should be taken to avoid this.

3. Case study: surface temperature effects

The previous section dealt with the selection of simulation parameters in order to ensure reasonable simulation results. These parameters are critical, but they are not

'experimentally-relevant'. Once a 'correct' set of parameters has been established they should not require further consideration. This section represents a case study of an input parameter that is experimentally accessible. In this case the factor under consideration is the sample temperature. This can be readily varied both in experiments and in simulations and consequently it allows for the possibility of cross-checking results and for testing the predictive qualities of simulations.

The sample temperature is typically one of the easiest parameters to control experimentally. It is also a parameter that can be critically important during etching. In particular it can influence the desorption rate of different species from the surface. During collision of CF-based species with silicon surfaces, atoms (C, F and Si) may be sputtered as a result of direct momentum transfer (pure physical sputtering), although in reactive ion etching (RIE) this mechanism plays a minor role. Alternatively, following dissociation some F atoms can react with Si or C atoms on the surface to form volatile products (such as CF_x or SiF_x species). These weakly bound groups may subsequently gain energy and be desorbed (chemically-enhanced physical sputtering) [103]. In this mechanism the main role of energetic ions is to remove products via the collision cascade that follows ion impact, while reactive C and F atoms play a role in weakening the bonding prior to sputtering. This process competes with spontaneous desorption of weakly bound products (chemical erosion) [104]. Spontaneous desorption is directly affected by the surface temperature. Any given species is more likely to desorb if the surface temperature is increased.

Downloaded At: 15:50 21 January 2011

Over the course of the simulations, atoms and clusters are removed from the surface at the end of each trajectory provided they satisfy one of two criteria, representing physical and chemical removal mechanisms, respectively. Clusters comprise groups of atoms. All atoms within the cluster have a separation from at least one other atom that is less than the cutoff value defined in relevant potentials and for which the potential between this atom pair is less then zero (attractive). The first criterion for desorption (physical sputtering) is fulfilled if the potential energy between the atom or cluster in question and the remaining atoms of the system is equal to or greater than zero (repulsive) and the particle has a velocity component directed toward the vacuum. The second criterion is met if the potential energy between the atom or cluster and remaining atoms is less than zero (attractive) but has an absolute magnitude that is less than a predetermined threshold energy. This threshold energy is related to the surface temperature.

In our simulations, for the evaluation of the second criterion a simple first-order thermal desorption model is used to predict if weakly-bound species will desorb spontaneously from the surface. When a cluster's binding energy with surface is smaller than a threshold energy computed from first-order thermal desorption theory [33], the cluster is considered to have desorbed from the surface. Species matching this criterion are removed from the simulation after each trajectory. The threshold energy is obtained from:

$$E_b = k_b T \ln(\tau \cdot A) \tag{20}$$

where k_b is the Boltzmann constant, T is the surface temperature, τ is a time constant (which is smaller than the real time that elapses before a subsequent molecule impacts) and A is a constant. Any molecule that is bound to the surface by less than this value is regarded as a desorbing species. Following the approach of Abrams and Graves [33], in our simulations we adopted $\tau = 1\,\mu s$ and $A = 10^{12}\,s^{-1}$. From Equation (20), the binding

energy threshold increases with increasing surface temperature (weakly bound species are more readily desorbed from the surface). If a species is found with a binding energy to the surface that is less than E_b, it is defined as desorbing as a result of chemical sputtering. On the purely technical level, the evaluation of the two criteria is done sequentially; the 'physical' criterion is evaluated first, followed by the 'chemical' criterion. All individual atoms and all possible cluster combinations are evaluated at the end of each trajectory. The fixed layers at the bottom of the simulated substrate provide the 'anchor' point for substrate atoms. All atoms that maintain a sufficient strong bond-chain to these layers remain on the surface.

In order to characterize the effect of sample temperature on etching (physical and chemical), test simulations, again for 100 eV CF_3 etching Si(100), were performed at sample temperatures of 100, 300, 600 and 800 K. Figures 10(a) and (b) show the predicted coverages of C and F atoms as a function of temperature over the course of the simulation. From the figure we note that, of the two incident atom types, the coverage of C atoms is most sensitive to the surface temperature. With increasing temperature, C-atom retention by the surface increases. In contrast, it is found that the coverage of F atoms is quite insensitive to the surface temperature. In the first instance, these results (particularly the increased uptake of C at higher temperatures) appear counter-intuitive. Since particles desorb more easily at higher surface temperatures, the opposite effect might be anticipated. The reason for the observed behaviour will become apparent from the additional simulation results presented in the following paragraphs. Briefly, it is due to a combination of increased CF_3 dissociation coupled with a low etch efficiency for deposited C. Figure 10(c) shows the etch yield of Si atoms as a function of exposure for the different surface temperatures. With increasing temperature, the etch yield increases. The steady-state etch rates are 0.199, 0.251, 0.275 and 0.373 for 100, 300, 600 and 800 K, respectively.

Downloaded At: 15:50 21 January 2011

Figure 11 shows a breakdown, as a function of temperature, of the Si etch yield into its chemical and physical components. The physical etching yield is greater than the chemical etching yield across the entire temperature range. This is unsurprising given the relatively high incident energy (100 eV) of the CF_3 molecules. As the sample temperature increases both the chemical and physical yields increase. The chemical etching yield increases by a factor of about 2, over the range studied, in an approximately linear fashion. The physical etching yield increases sharply from 100 to 300 K, but above 300 K, the increase is more gradual.

Figure 12 shows the atomic densities in the sample as a function of depth for samples held at 300 and 800 K after exposure to 40 ML of 100 eV CF_3. It can be seen that with increased substrate temperature, the peaks of C and F shift somewhat toward the bulk (a result of the increased etch rate). Compared with the 300 K sample, the reaction layer formed at 800 K is broader and, within this reaction layer, both the C and F distributions are broader. Despite the enhanced etching at 800 K, Si persists out to the outermost surface region in the reaction layer formed. The increased Si removal is reflected in a more gradual increase in Si density going toward the bulk crystal.

Figure 13 shows the yield of some of the critical Si products (SiF_x; $x = 2$–4), produced by etching, as a function of temperature. From the figure, we note that the yields of SiF_2 and SiF_3 are most strongly dependent on the surface temperature, while SiF_4 is relatively insensitive. With increasing temperature, the yields of both SiF_2 and SiF_3 increase, while

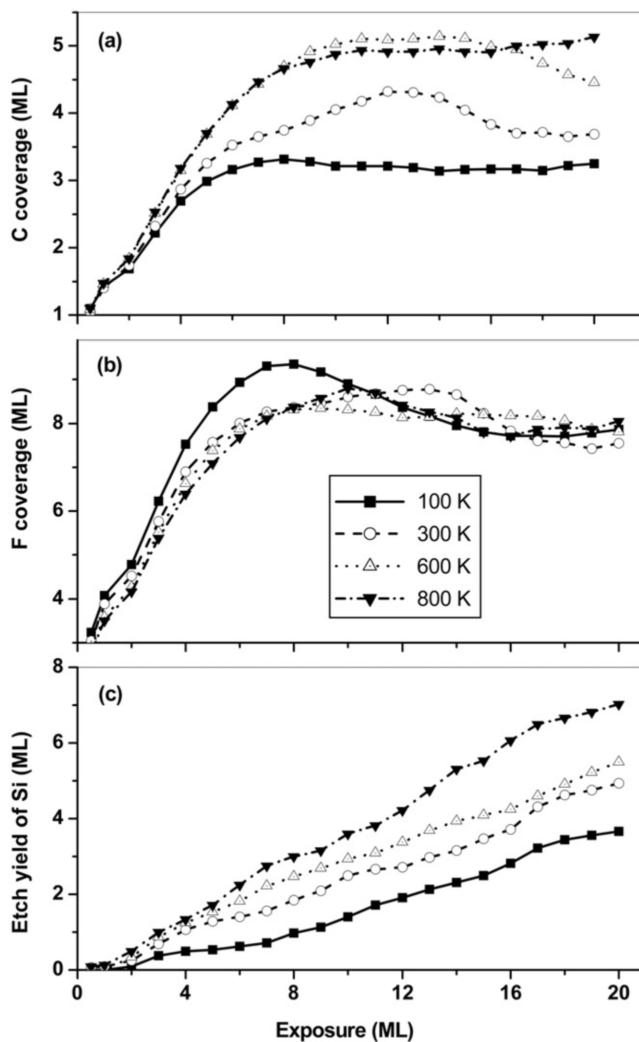

Figure 10. Coverages of (a) C and (b) F atoms on the Si sample as a function of exposure to 100 eV CF_3 for different sample temperatures; (c) Si etching yield as a function of the exposure.

the yield of SiF_4 remains effectively constant. At the lowest temperature, the yield of SiF_4 is greater than that of SiF_2 or SiF_3, while the yield of SiF_2 is the smallest of the three. As the temperature increases, SiF_3 becomes the dominant etch product. At 800 K, the yield of SiF_2 is close to that of SiF_4, while the yield of SiF_3 is almost twice that of SiF_2. The difference is primarily due to the increased binding energy required in order for a volatile species to remain on a surface when the temperature is elevated. In the case of SiF_4, because all atoms in the molecules have their bond-order requirements fully satisfied, the interaction with the surface is very weak. Such a molecule will only remain on the sample if the temperature is extremely low, or if the molecule is formed relatively deep in the substrate and, as a consequence, is sterically prevented from desorbing. Hence the

Downloaded At: 15:50 21 January 2011

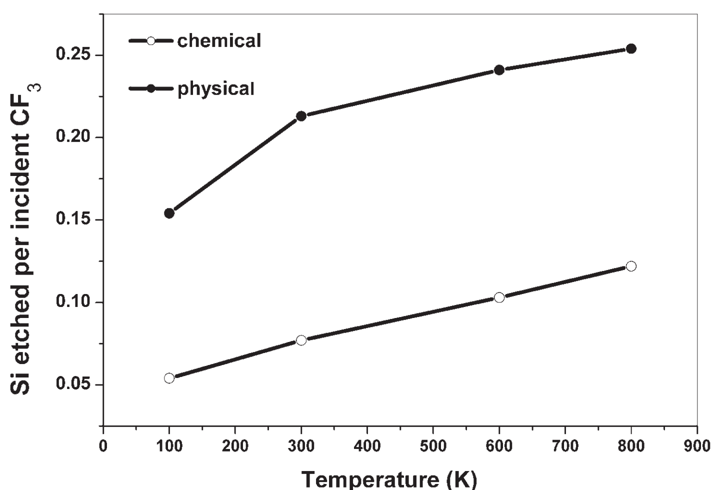

Figure 11. A breakdown of the chemical and physical Si etching yields as a function of sample temperature for Si(100)-2 × 1 exposed to 100 eV CF_3.

Downloaded At: 15:50 21 January 2011

yield of SiF_4 is relatively independent of the sample temperature (directly) but is critically dependent on the number of precursor (–SiF_3) species present on the surface. The relatively constant yield predicted in Figure 13 illustrates that the standing coverage of –SiF_3 is virtually unchanged at the different temperatures despite the higher desorption of both SiF_2 and SiF_3.

In the case of SiF_3 and SiF_2, these molecules can maintain 1 and 2 bonds, respectively, with the surface atoms and are consequently less prone to spontaneous desorption. Given that SiF_2 can bind more strongly to the surface than SiF_3, the relative trends of the traces shown in Figure 13 are self-explanatory. These trends will only be broken when the desorption efficiency of SiF_2 becomes sufficiently high that it reduces the standing coverage of –SiF_2 groups (and thus interrupts the production of SiF_3 groups).

Figure 14 shows the cumulative yields of all ejected products, including those arising from scattering of the incident molecules, at different sample temperatures. From the figure we note that with increasing temperature, the yield of F increases, the yield of CF remains effectively constant and the yields of CF_2 and CF_3 decrease slightly. The yields of larger molecules C_xF_y ($x > 1$, $y > 0$) and $Si_xC_yF_z$ ($x, y, z > 0$) are effectively constant as a function of temperature. The increase in the amount of F atoms leaving the surface indicates more CF_3 dissociation is occurring at higher surface temperature (the reaction probability has increased). There is also an increased production of Si-containing species at higher temperatures. Figures 13 and 14 combine to reveal illustrate a higher turnover of F atoms at higher temperatures.

Considering the C-containing species that are found to leave the surface, the bulk of these arise as a result or direct or dissociative scattering (CF_4; CF_x ($x = 0$–3)). Most of the remaining C-containing fragments are ejected as a result of direct physical sputtering. F atoms released from the incident molecules react preferentially with Si atoms. Hence, chemical etching processes tend only to remove C atoms when they are incidentally attached to a larger Si-containing group. The tendency of C atoms to persist on the

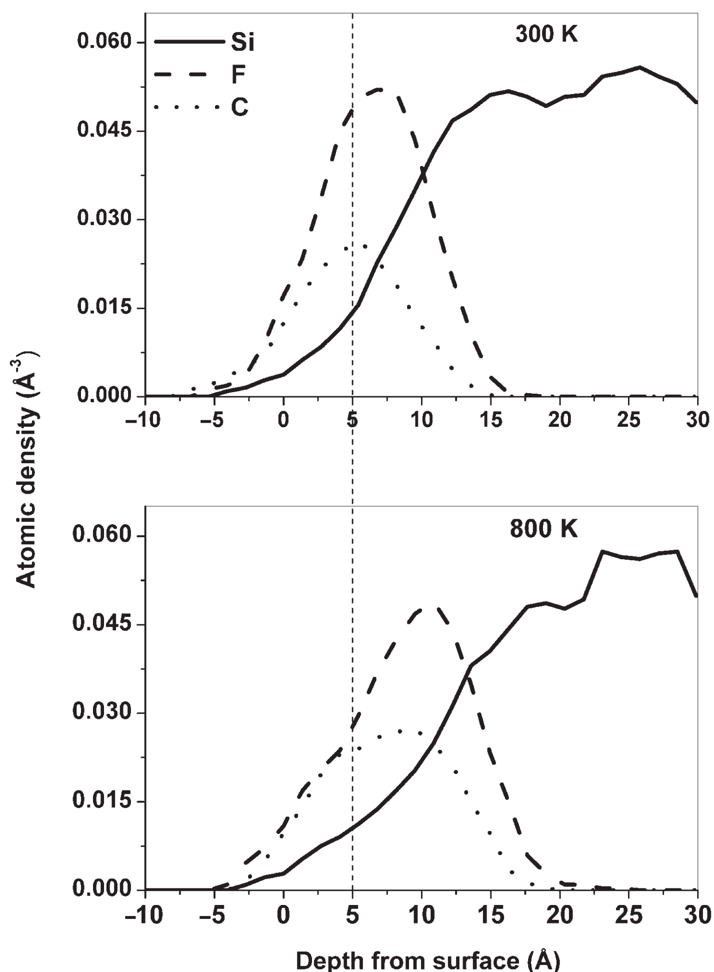

Figure 12. Atomic densities in the sample as a function of depth after 40 ML exposure to 100 eV CF_3 at sample temperatures of 300 and 800 K.

Downloaded At: 15:50 21 January 2011

surface coupled with the increased dissociation at higher temperatures leads to the increasing coverages as a function of temperature seen in Figure 10(a). The effect saturates once the combination of incident energy and surface temperature results in C being extracted from the incident molecules at close to the maximum efficiency.

Figure 15 shows a detailed comparison of the yield-per-incident CF_3 of the SiF_2, SiF_3 and SiF_4 etch products as a function of exposure at 300 and 600 K. For both temperatures, during the initial stages the yield of SiF_2 increases sharply, reaches a maximum and then decreases toward a steady-state. For SiF_3 and SiF_4, the yields increase more gradually as the simulation processes and then reach their steady-states. These species have very weak or no maxima in their yield as a function of exposure. The variation in yield-per-CF_3 of the different products reflects the different exposures required to produce the relevant precursor groups on the surface. Significant production of SiF_2, SiF_3 and SiF_4 require SiF,

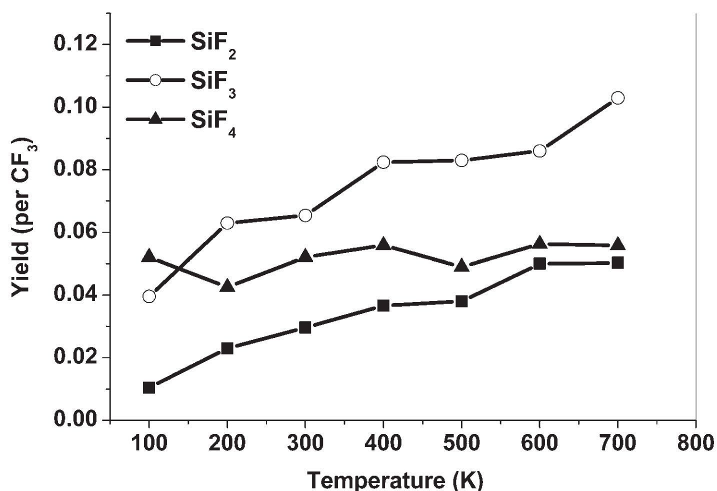

Figure 13. Yield of the major Si etch products as a function of sample temperature for 100 eV CF_3 incident on Si (100)-2 × 1.

Downloaded At: 15:50 21 January 2011

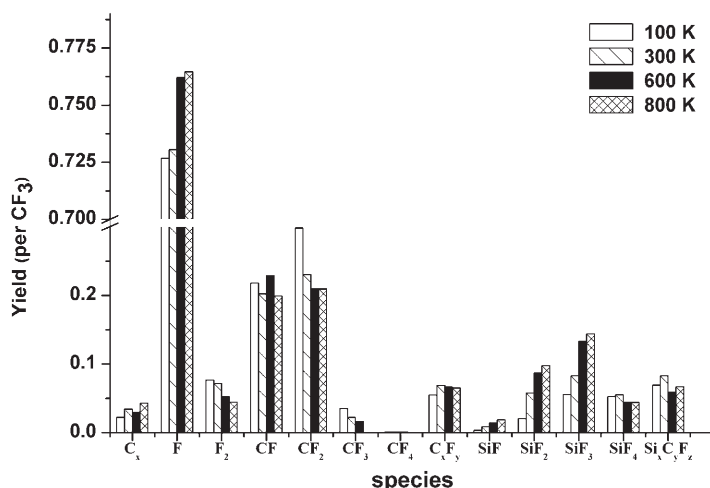

Figure 14. Yield of all ejected products, including those arising from the incident molecules for 100 eV CF_3 incident on Si (100)-2 × 1 at different sample temperatures.

SiF_2 and SiF_3 functional groups, respectively, to be present on the surface. Hence, at low exposures (less than 12 ML) the yield of SiF_2 is greater than that of SiF_3. After ~12 ML exposure, the yield of SiF_3 becomes the largest. At 300 K, when the yield of SiF_2 reaches its maximum, SiF_3 and SiF_4 molecules start to appear, while at 600 K, SiF_2 and SiF_3 are produced simultaneously. After 2.5 ML exposure, SiF_4 molecules start to emerge. Over the course of the simulations at 300 and 600 K, the yield of SiF_4 always remains the lowest. The relative ease with which SiF_3 can be induced to leave the surface prevents the formation of a large standing coverage of SiF_3 functional groups (SiF_4 precursors) in the

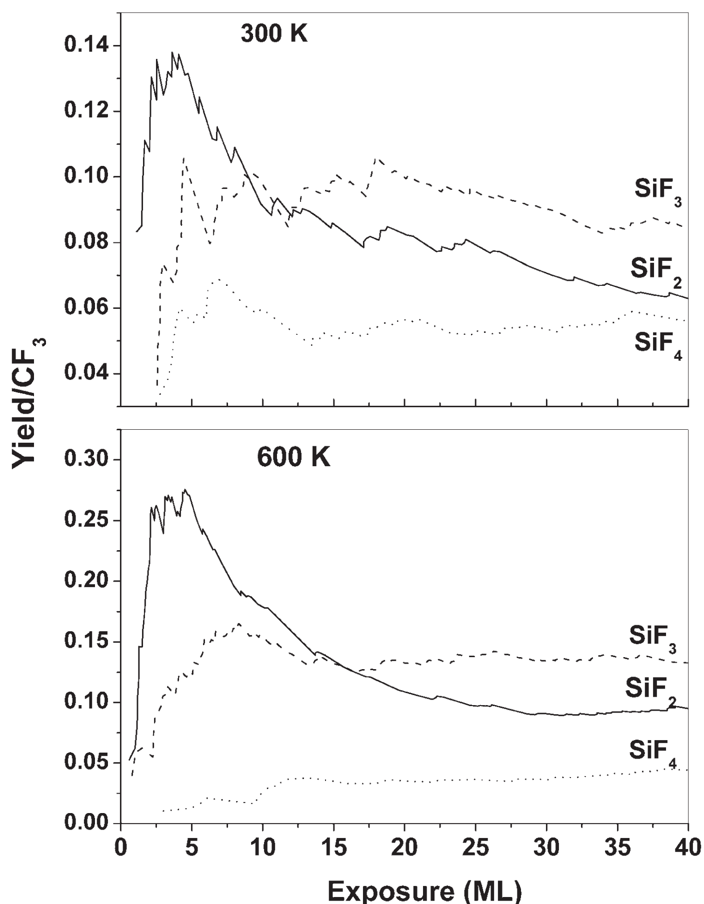

Figure 15. The yield-per-CF_3 of SiF_2, SiF_3 and SiF_4 etch products as a function of exposure to 100 eV CF_3 at sample temperatures of 300 and 600K.

Downloaded At: 15:50 21 January 2011

reaction layer. With increasing temperature, the steady-state coverage of F atoms is not significantly changed (as shown in Figure 10b), while the yield of F-containing Si etch products increases. Hence, even though the standing coverage does not change, there is a higher turn-over of F atoms at the higher temperatures. This occurs through more effective extraction of the available F-atoms from the incident molecules, which is also reflected in the increased uptake of C atoms by the surface (see Figure 10).

In our simulations, with increasing substrate temperature the etch yields of SiF_2 and SiF_3 increased, while the yield of SiF_4 was almost independent of the substrate temperature. The etching rate increases from 0.199 to 0.373 when the temperature is increased from 100 to 800 K. Both physical and chemical erosion mechanisms are enhanced by elevating the sample temperature, with the chemical process showing the greatest enhancement in relative terms. The increased Si etch yield is mainly contributed by increased desorption of SiF_2 and SiF_3 molecules. This behaviour was observed experimentally by Winters and Coburn using mass spectrometry during Si etching by

XeF_2 [11]. In their experiments they observed that when the substrate temperature was increased from room temperature to 600 K, Si etching was enhanced and SiF_2 species were desorbed. Sebel *et al.* performed Ar^+-assisted Si etching by XeF_2 in the temperature range $T = 150–800$ K [105]. They also reported that the etch rate was enhanced with increasing substrate temperature. A number of experimental studies have demonstrated that the substrate temperature affects the desorbing species during etching [11,106]. Humbird and Graves performed MD simulations of spontaneous etching of silicon by F atoms as a function of surface temperature and have reproduced similar behaviour [39,107]. These authors propose that at higher temperatures the SiF_x layer begins to spontaneously decompose to produce SiF_2 species that desorb from the surface. They also point out that since MD simulation can only capture events on the picosecond time-scale, the simulations will tend to underestimate the production of SiF_2 species relative to the experimental results. (This underestimation should also present in our simulations.) For 100 eV CF_3 bombardment (current work) SiF_2 species are not the main product. In the simulation, we impinge 100 eV CF_3 molecules one after another with no interval time between two sequential impacts. In reality, the typical impact interval on such a sample area would be on the order of a millisecond. Therefore, in the simulations spontaneous decomposition of SiF_2 species is limited as a consequence of the high impact rate. The short time between impacts results in an increase in the probability of SiF_3 formation versus SiF_2 desorption.

Downloaded At: 15:50 21 January 2011

4. Plasma–surface interactions

This section outlines some of the main results and conclusions that have been derived for PSI-relevant MD simulations. It is by no means exhaustive, but it will provide a good starting point from which to approach the field. We will cover the general mechanism that have been proposed as well as come of the specific results generated.

4.1. *Mechanisms of PSI*

When species (such as radicals and ions) in plasmas interact with silicon, a number of chemical and physical events may occur, depending on the bombarding species, the flux and the energy. Neutral radicals will have a low kinetic energy, determined by the plasma temperature. In contrast, ions approaching a surface will experience acceleration due to the presence of a sheath potential. To completely understand the physics and chemistry involved, it is important to understand the various interactions both in isolation and in concert. When only radicals impact on a silicon surface, they may be reflected away from the surface after experiencing some energy loss or they may be adsorbed on the surface via chemical reaction or physisorption, due to their relatively low kinetic energy. In contrast, when only ions impinge on the surface the acceleration across the sheath potential results in a much more significant collision cascade. Some translational energy is transferred from the incident ions to the surface and the near-surface region and may results in a variety of processes including:

(1) A local thermal spike that promotes diffusion and creates phonons that may supply the activation energy required for bond cleavage;
(2) direct bond-breaking to create dangling bonds, including possible sputtering and abstraction events;

(3) for chemically reactive molecular ions, reaction (possible coupled with fragmentation) with surface atoms resulting in adsorption, implantation or nucleation;
(4) collision-induced desorption of physi- or chemisorbed species;
(5) sputtering and/or displacement of atoms in the surface or near-surface region [108].

Three mechanisms have been proposed to explain material erosion in the presence of reactive ions. The first mechanism is chemically-enhanced physical sputtering, proposed by Mauer *et al.* [103] for reactive ion etching of Si by a CF_4 plasma. It suggests the formation of volatile products (SiF_x) that are more weakly bound to the surface than unreacted Si and are thus more susceptible to physical sputtering. The second mechanism, proposed by Tu *et al.*, is called chemical sputtering [104]. It suggests that ion bombardment induces a chemical reaction producing weakly bound molecules that can spontaneously desorb from the surface. In the specific case studied by Tu *et al.* (Ar^+ and XeF_2 incident on Si and SiO_2), they proposed that the incident species induce a reaction between Si and adsorbed F, leading to the formation and subsequent desorption of SiF_4. The third mechanism, which was originally suggested by Coburn *et al.* and later expanded upon by Flamm and Donnelly, is characterized as a damage-induced chemical reaction [109,110]. It proposes that the lattice damage caused by ion bombardment results in enhancement of a chemical reaction on the surface relative to the reaction rate on the undamaged material.

Downloaded At: 15:50 21 January 2011

When ions impinge on the silicon surface in the presence of fluorine or fluorine-based molecular radicals, the phenomena occurring are complex. Figure 16 illustrates this complexity. This figure was produced by Humbird and Graves to present the lifecycle of Si under bombardment by CF_2 and F at thermal energies and Ar^+ at 200 eV [58]. The bombardment produces a layered structure consisting of a Si–C outer layer above a Si–F region. The SiF and SiC layer were found to move through the substrate with Si being removed as part of the etch products. The argon ions play a variety of roles in the

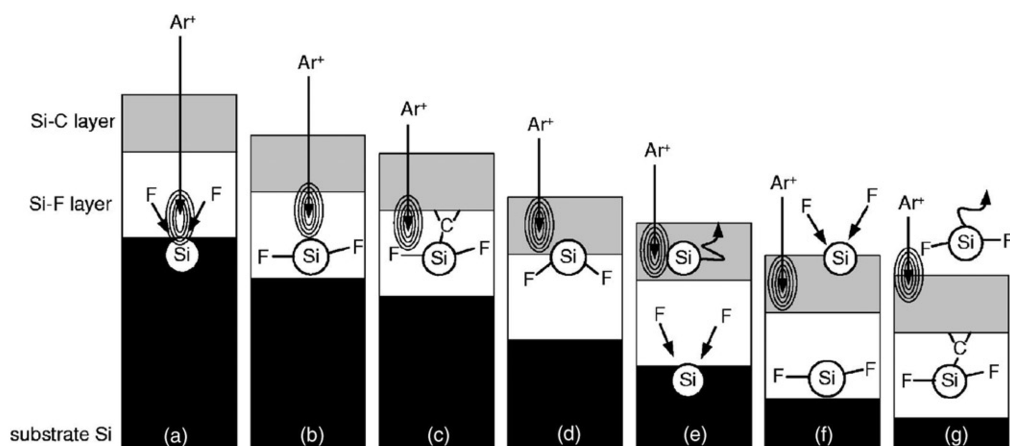

Figure 16. The Si lifecycle as deduced from the simulation results of $CF_2:F:Ar^+$ bombarding silicon. (Reused with permission from David Humbird, Journal of Applied Physics, **96**, 2466 (2004). Copyright 2004, American Institute of Physics.)

concerted etching process The ions may deposit their energy at different regions in the surface generating the range of processes illustrated in the figure. The main processes identified were: (a) mixing F into the Si substrate (extending the SiF layer), (b) disrupting the SiF layer (enhancing mobility), (c) disrupting the SiC–SiF interface (advancing the SiC layer), (d–f) disrupting the SiC layer ('de-fluorinating' the SiC and transporting Si to the surfaces where it can react with F atoms) and (g) collision induced desorption of atomic and molecular species from the surface. The Si–C layer formed near the surface region acts as an etch inhibitor. However, the impact of the Ar^+ ions ensured that there is sufficient mobility of F and Si through this layer to maintain an etching mechanism while sustaining the layer structure.

Humbird and Graves also discussed the mechanisms of Ar^+-assisted etching of silicon by F and Cl [107]. They concluded that two mechanisms (chemically enhanced physical sputtering and chemical sputtering) play an important role in etching. Ion-assisted etching is interpreted as chemical sputtering. Chemical reactions induced by the ion collision cascade create weakly bound SiF_x products. These weakly bound species can leave the surface during or promptly after the impact. In the simulation, chemically-enhanced physical sputtering is defined as a mechanism where etching products are created promptly after impact. For the case of 100 eV Ar^+ and a F/Ar^+ ratio of 5, the calculations demonstrate that 27% of the ion-assisted etching is attributable to chemically-enhanced physical sputtering, the remainder is from chemical sputtering.

Barone and Graves used MD simulations to investigate characteristics of chemical and physical sputtering of fluorinated silicon [35]. In their simulations, fluorinated reaction layers with varying F/Si ratios were fabricated by bombarding the silicon surface with F. These layers were then subjected to energetic Ar^+ bombarding. They concluded that at low F/Si ratio (F/Si <0.5) only enhanced physical sputtering was observed. However, at ratios of F/Si >0.5 in the fluorinated layer a chemical sputtering mechanism appeared to be dominant.

In our studies of 100 eV CF_3 interacting with silicon surfaces F atoms play two roles. During the collision cascade, F atoms react with Si atoms to weaken the binding to the surface. Simultaneously, F and C atoms transfer some of their momentum to the surface atoms and induce physical sputtering. The energy deposited by CF_3 incident molecules in the layer was concentrated near surface region [35]. The deposited energy may be used to redistribute F atoms from the surface to deeper layers where they can react with Si atoms and subsequently to transport the resulting SiF_x to the surface. Relative to the thermal desorption energy, for molecules incident at 100 eV the energy deposited around the impacting site is very large. Therefore, at 100 eV pure chemical sputtering is limited and the chemically enhanced physical sputtering mechanism is dominant.

4.2. *Species effects*

Fluorocarbon plasmas consist of many types of CF_x species and reactive ions (F^+, CF^+, CF_2^+, CF_3^+). In addition, etched products (SiF_x; $x = 1$–4) can be ionized and return to the surface. Therefore, systematic investigation of how these neutral species and ions interact with the Si surface is useful. The following is a brief overview of some of the work that has been done on relevant systems.

Downloaded At: 15:50 21 January 2011

Downloaded At: 15:50 21 January 2011

4.2.1. *F Radical*

The interaction of F with silicon surfaces is of great importance during etching, and thus has been intensively studied via experiments and simulations [11,39,49,60,83,111–125]. Experimental data shows that as the F exposure increases, a fluorinated reaction layer consisted of SiF_x ($x = 1$–3) is formed [11]. The formation of this layer results in spontaneous etching at room temperature. When Si(111) bombardment by F atoms with energies in the range of 0.1–1 eV was simulated by Gadiyak *et al*. [113], the F atoms were found to always saturate dangling bonds forming SiF_x species. For impacting F_2 molecules they also found that, with adsorption on the silicon surface, F_2 dissociates due to the release of the Si–F bond formation energy. Both of the released atoms may adsorb on the surface or one may scatter away. Humbird and Graves investigated spontaneous etching of silicon by atomic fluorine using their improved Tersoff–Brenner type potential [39]. At 300 K, the simulated etch probability, defined as the number of silicon atoms removed per incident F atoms, was 0.03, which is in good agreement with many experiments [114,126]. The simulations show that the primary etch products are SiF_4 (71%), Si_2F_6 (27%) and Si_3F_8 (1%). Smaller clusters (SiF, SiF_2, SiF_3) represented less than 1% of the etch products. These findings directly supports the assumption by Winters and Coburn that in experiment most of SiF_2 etch products arise from cracking of Si_2F_6 and only a very small amount of SiF_2 is formed directly [11]. The calculations predict that the most likely kinetic energy for SiF_4 is about 0.2 eV, while for Si_2F_6 the most likely kinetic energy is about 0.1 eV.

4.2.2. *Ar^+ ion*

Under Ar^+ bombardment, an initially crystalline surface will become amorphousized. Graves and Humbird performed simulations to investigated energetic Ar-ion induced amorphousization and recrystallization of Si [56]. Under bombardment an amorphous layer is established in the outermost region of an initially crystalline lattice. Once formed, the thickness of the amorphous layer was characteristic of the incident energy used and was found to be maintained by a kind of dynamic balance. The result implies an ability to recrystallize a sample by reducing the ion energy. Figure 17 shows the ion-induced amorphous silicon and subsequent recrystallization that they induced via ion energy control. From the figure, a steady-state amorphous layer with a thickness of $\sim$18 Å is established under 200 eV Ar^+ bombardment. The authors then reduced the incident energy in a step-wise fashion to 100, 50, 20 and 10 eV respectively. At each step the amorphous layer thickness tended to stabilize at a lower value as a result of lattice recrystallization. It was found the ion energy had to be reduced in the controlled fashion shown in order to induce rapid recrystallization. Changing from 200 eV directly to 20 eV resulted in a much slower process. This was attributed to the requirement to deposit sufficient energy near the amorphous–crystalline interface in order to induce atomic rearrangement. Too high an energy will maintain a thick amorphous layer, too low will mean that too few ions will reach the boundary region and recrystallization will be very slow.

4.2.3. *F^+ ion*

Aoki *et al*. investigated the impact processes of fluorine atoms, molecules and clusters ($(F_2)_{30}$). Their results for 50 eV F^+ bombarding silicon surfaces show that F atoms saturate

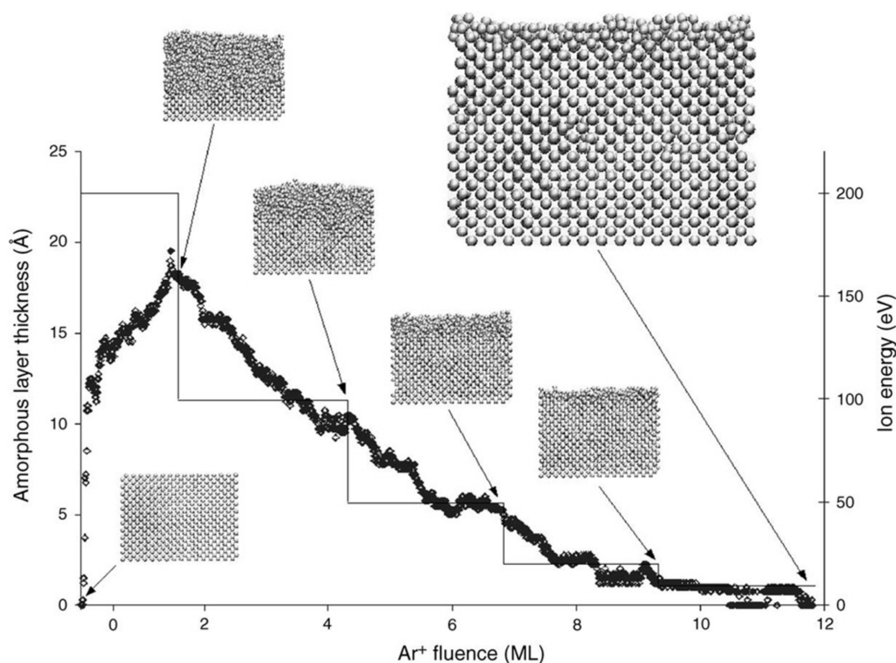

Figure 17. Plot showing amorphous silicon layer thickness as a function of Ar^+ fluence as ion energy is changed (solid line). The approximate amorphous layer thickness (left axis) decreases from ~18 to ~2 Å as the ion energy (right axis) is reduced stepwise from 200 eV to 10 eV. (Reprinted from Applied Surface Science, 192, D.B. Graves and D. Humbird, *Surface chemistry associated with plasma etching processes*, 72–87, Copyright (2002), with permission from Elsevier.)

Downloaded At: 15:50 21 January 2011

silicon bonds and weakly bound SiF_x species are formed near the surface region [127]. In the case of incident F atoms or molecules, they found that removal of Si does not occur for energies less than 10 eV/atom and the incident species are merely adsorbed on the surface. However, even at 1 eV/atom F_2-clusters can produce etching via chemical desorption of SiF_x species. With increasing incident energy, the ratio of fluorinated to non-fluorinated species leaving the surface decreases. At high energy (100 eV/atom) the clusters removed large amounts of unfluorinated Si atoms and clusters via sputtering. At low energies a fluorinated Si surface was more resistant to etching/sputtering than bare Si.

4.2.4. CF_x^+ *ions*

Toyoda *et al.* investigated energy-controlled and mass-selected CF_3 ions interacting with Si surfaces experimentally [128]. They measured the time evolution of neutral radicals desorbing from the surface by appearance mass spectrometry. The yield of CF_2 increased monotonically with exposure to CF_3 until a steady-state was reached. They found that the SiF_2 desorption reached its maximum at about 3 ML exposure. Subsequently, the SiF_2 desorption decreased and reached a steady-state after about 40 ML exposure.

Abrams and Graves systemically simulated CF_x ions bombarding amorphous silicon surfaces [30,33]. For CF_3 ions, they obtained a steady-state etch yield comparable to experimental data [129,130]. Comparisons with available experimental data demonstrate that their new TB-form potentials could qualitatively predict the etching dynamics on the atomic level. Similar to F bombardment, CF_3 exposure results in a fluorine-rich reaction layer being formed on the surface, through which a balance between deposition and removal of C and F atoms is established. The thickness of the reaction layer increases with increasing CF_3 incident energy. For simulations involving CF and CF_2, their results showed a C-rich layer being formed rather than a F-rich layer. A transition from net fluorocarbon deposition (for CF) to net Si etching (for CF_3) is predicted. This was due to the increased number of F atoms per incident particle when switching from CF to CF_3. During interaction with the silicon surface, these molecular ions can dissociate to produce free F atoms. These atoms can react with Si atoms to form weakly-bound SiF_x species and may lead to etching. Simulations of energetic CF bombarding silicon surfaces performed in our group predict formation of silicon carbide near the surface region [92]. Jang and Sinnott simulated CF_3^+ and $C_3F_5^+$ bombarding a polystyrene surface. Their simulations predict that CF_3^+ is most effective at fluorinating the surface (a prerequisite for etching) [40]. In contrast, $C_3F_5^+$ was judged to be more efficient at growing fluorocarbon thin films due to long-lived CF_2 being the dominant fragment produced.

Downloaded At: 15:50 21 January 2011

4.2.5. *SiF_x^+ ions*

As part of their efforts at elucidating the surface chemistry of plasma etching processes, Graves and Humbird performed MD simulations of SiF_3^+ bombarding a silicon surface at 100 eV and normal incidence [56]. This is analogous to an ionized etched product being redeposited on a plasma-facing surface. Figure 18 show the resulting uptake of Si and F from impacting SiF_3^+ and the corresponding etching of the original silicon atoms as a function of ion fluence. The inset on the figure shows the atomic configuration at the end of the simulation. The bombardment results in the formation of a deep crevice on the surface. F atoms were not found to intermix appreciably into the substrate, whereas ‘redeposited’ Si atoms were well mixed with the original silicon in the reaction layer. As a consequence, steady etching of the original Si was observed even in the presence of significant new Si deposition. The resulting surface was similar to those obtained for F bombarding pure Si. Due to the intermixing, the ‘redeposition’ of ‘etched’ products does not hinder the etching of the original substrate atoms.

Helmer and Graves investigated SiF_x ($x=0$–3) impacting fluorinated silicon surfaces with energies ranging from 0.1 to 100 eV. In their simulations, the effects of sticking, reflection or dissociation of the impacting species, reactions with surface species and sputtering of the surface on the incident angle was studied in detail [38]. The authors noted the complexity of the system, where the results obtained are critically dependent on the chemical composition of both the incident and surface species as well as the angle of incidence and the incident energy.

4.3. *Synergistic effects*

Many experiments have demonstrated that ions play an important role in etching. The synergistic effect of chemically active radicals and energetic ions in plasma was

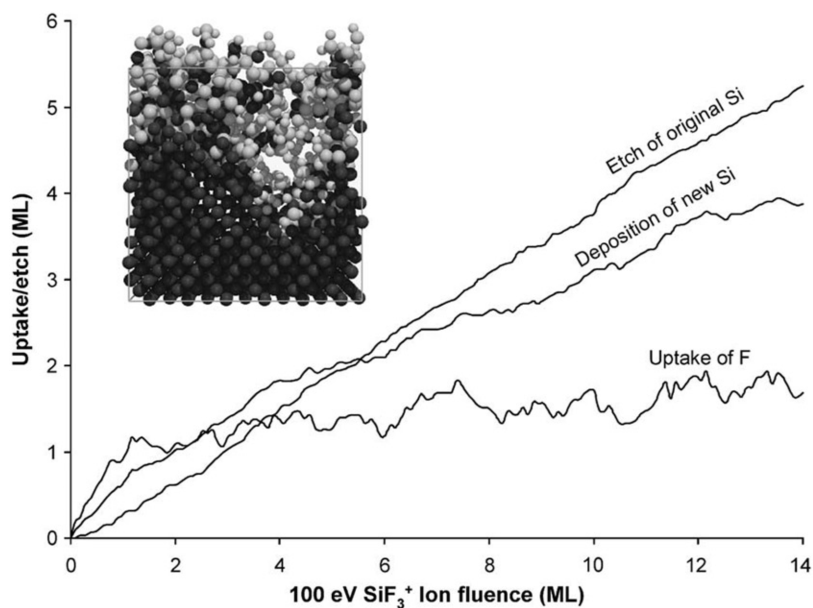

Figure 18. Fluorine uptake and silicon etch and deposition plots for Si bombarded by SiF_3^+ at 100 eV. The final atomic configuration is shown in the inset. The small atoms are F, the large atoms are the original Si (dark), and deposited Si (light). (Reprinted from Applied Surface Science, 192, D.B. Graves and D. Humbird, *Surface chemistry associated with plasma etching processes*, 72–87, Copyright (2002), with permission from Elsevier.)

Downloaded At: 15:50 21 January 2011

initially investigated by Coburn and Winters for the combination of XeF_2 gas and Ar^+ etching amorphous silicon [11,131]. In their experiment initially XeF_2 only, then XeF_2 and 450 eV Ar ions together and finally only 450 eV Ar ions were exposed to the surface. Figure 19 shows the measured etch rate during the various exposure periods. This experiment unambiguously demonstrated the synergistic effect. The etch rate of the combination of XeF_2 and Ar^+ is much greater than for either of the species individually. Humbird and Graves also demonstrated a synergistic effect during simulations of F and Ar^+ bombarding a Si surface [107]. Figure 20 shows the F uptake and surface SiF_x species distribution as a function of F fluence both in the absence and presence of 200 eV Ar ion bombardment. In their simulations, after the surface is exposed to F atoms, a steady-state coverage of SiF_x species is quickly established. When this surface was bombarded simultaneously with F and 200 eV Ar^+ ion the uptake F increases substantially and the coverage of SiF_x species in the surface changes. In particular, there is a dramatic increase in the amount of SiF on the surface and a decrease in the coverage of SiF_3. The simulation results indicate that ion-induced mixing plays a primary role in enhancing the etch rate of Si atoms in the presence of F.

Results for CF_2, F and Ar^+ impacting silicon surfaces showed that a silicon carbide surface layer above an F-rich layer is formed as shown in Figure 21 [58]. In these simulations, the kinetic energies of the thermal species (CF_2 and F) were chosen from a Maxwell–Boltzmann distribution around 300 K, while the Ar ions were incident at 200 eV.

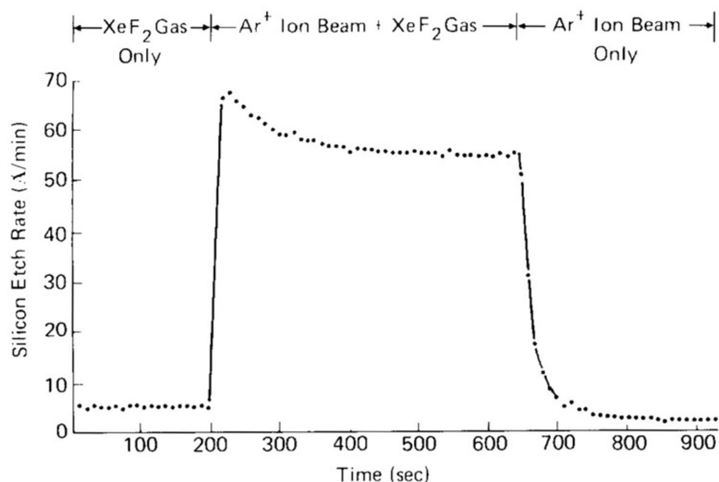

Figure 19. Silicon etch rate as a function of time for exposure to XeF_2 (0–200 s), combined Ar^+ and XeF_2 (200–650 s) and Ar^+ (>650 s). (Reprinted from Surface Science Reports, 14, H.F. Winters and

Downloaded At: 15:50 21 January 2011

As shown in Figure 21 a layered structure emerges, with an SiC outer layer, then an SiF_x layer, and amorphous Si layer and finally the original ordered Si structure. The SiC and SiF_x layers were formed as a result of Ar ion impact and ion-induced mixing. Carbon in the SiC layer raises the total atomic density and acts as an etch inhibitor by preventing Ar ions from reaching the SiF layer. The Ar^+ energy remaining after penetration of the Si–C layer directly determines the etch yield. If the SiC layer grows sufficiently thick to prevent the ions reaching the SiF layer, etching ceases. This work was extended by Végh *et al.* [132] who studied Si etching in the presence of fluorocarbon species (CF and C_4F_4), F atoms and Ar^+. The aim was to determine suitable conditions that would permit steady-state etching in the presence of a fluorocarbon film. By selection of a suitable set of input parameters it was possible to achieve this. Of primary importance was the presence of a FC species with suitably high sticking probability. This ensured the formation of a porous film structure, allowing continued transport to and from the underlying Si. It was concluded that ion-assisted processes consisted of (1) ion energy deposition, (2) ion-induced mixing and (3) reaction promotion.

4.4. *Surface composition and structure*

The surface composition and structure can influence the outcome of Si etching. In addition, the etching process will be influenced by chemical modification of the surface prior to or during the actual etching. Several studies have been performed on the etching of fluorinated silicon surfaces. Barone and Graves simulated fluorinated silicon surfaces under bombardment by energetic Ar (20, 50 and 200 eV) [35]. They found that for low F content (<50%) only physical sputtering was predicted, but with a higher yield than that observed for pure amorphous silicon. At higher F contents, the ion

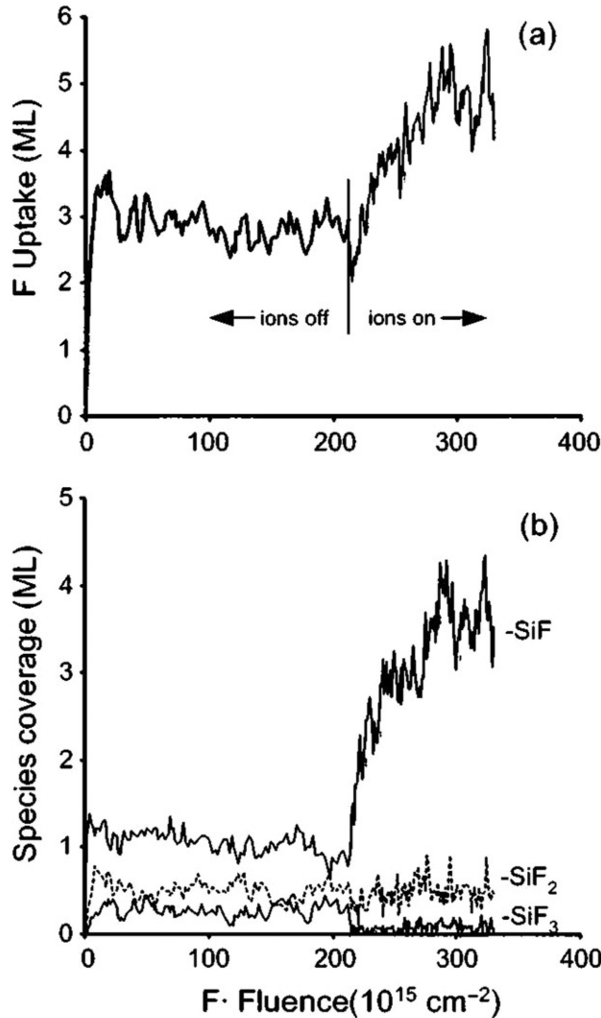

Figure 20. Change in (a) total F uptake, (b) surface species coverage as a result of F bombardment in the absence (<210) and presence (>210) of 200 eV Ar ions ($F:Ar^+$ ratio = 5 : 1). (Reused with permission from David Humbird, Journal of Vacuum Science & Technology A, **23**, 31 (2005). Copyright 2005, AVS The Science & Technology Society.)

Downloaded At: 15:50 21 January 2011

impacts resulted in the formation of SiF_x species in the layer, analogous to chemical sputtering.

To elucidate the role of fluorocarbon surface layers formed during ion-assisted etching, we have simulated CF_3 ions bombarding silicon surfaces covered by a fluorocarbon (FC) layer formed prior to bombardment [133]. It was found that the composition of the reaction layer is dynamic during etching. The steady-state reaction layer is continuously renewed by the incident CF_3 ions. Compared with the bare Si surface the etch rates are significantly decreased in the presence of the FC layer. Végh *et al.* also reported that the etch rates decrease with increasing FC layer thickness [132]. This is due to the presence of

Downloaded At: 15:50 21 January 2011

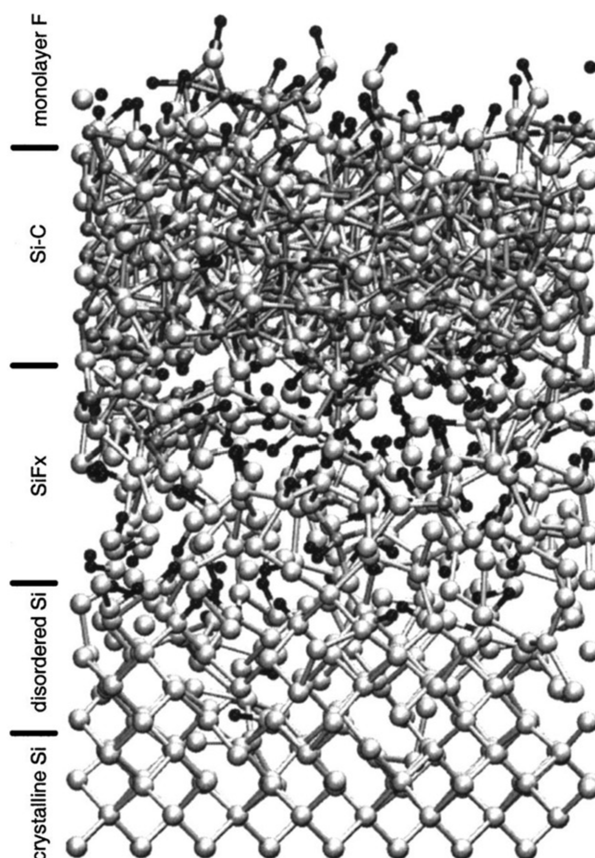

Figure 21. Side view of layered structure generated by bombarding a Si surface with CF_2 and F (both at thermal energies) and Ar^+ at 200 eV. Ratio of $CF_2 : F : Ar^+ = 7 : 2 : 1$. (Reused with permission from David Humbird, Journal of Applied Physics, **96**, 2466 (2004). Copyright 2004, American Institute of Physics.)

FC layers hindering etchants from penetrating into the deeper layers and retarding products leaving the surface. If the FC film layer deposited is hard, dense and cross-linked, no steady-state etching is established and the etching eventually ceases. When a sufficiently open and porous FC layer is grown (via selection of appropriate FC species), it was possible to maintain steady-state etching in the presence of an FC layer. Therefore, the FC layer can have a significant influence on Si etching.

In addition to composition, the surface structure also plays a determining role in etching. Humbird and Graves found that the etch rate on the amorphous silicon is about 70% higher than on the crystalline Si surface [107]. This is due to the more open structure of the amorphous surface. However, structural effects will ultimately be transitory since the etching process will tend to impose its own steady-state structure on the sample. In some cases the effect of etching will be the formation of a ‘passivation’ layer resulting in the cessation of the etching process and the creation of a new ‘stable’ surface with an altered composition and structure.

5. Concluding remarks

We have attempted to give an overview of the application of classical molecular dynamics to the study of PSI-relevant systems, particularly CF_x containing plasmas interacting with Si-based surfaces. Both the practical aspects of implementing the simulations and a consideration of the typical results obtained have been provided. We have discussed the effects of the temperature control (the application time of the heat bath, the rising time), the relaxation time of the (post-) bombarded sample, the cell size, the time-step and the integration time on the etching. The simulation results show that the heat-bath application time and the cell size have the greatest effects. The other factors have no major influence on the etching (within the parameter range investigated).

The effects of the substrate temperate on etching have been investigated in detail. With increasing substrate temperature, the etching rate increases, which is in good agreement with the available experimental results. The increased etch yield with increasing temperature is mainly due to the increased desorption of SiF_2 and SiF_3 species. The composition of the desorbing species is critically dependent on the sample temperature. However the standing coverage of SiF_x species is less dependent on the temperature because the increased desorption rate at higher surface temperatures is compensated for by a higher turnover of F atoms from the incident CF_3 molecules.

The range of processes that can occur during PSI is already well established. However, the relative importance of the different mechanisms is critically dependent on the precise energies and chemical composition of the plasma. The precise chemical species that are incident on the surface and the composition of the surface play a crucial role in determining the outcome. In particular, the existence of synergistic effects can result in dramatic changes to the process by means of relatively minor modification of the plasma. Hence, fully characterizing the plasma parameter space will enable enhancement and optimization of the control of plasma processing.

Downloaded At: 15:50 21 January 2011

Acknowledgements

We would like thank to Prof. B. J. Thijsse (Delft University), Prof. W. Goodheer (FOM-Rijnhuizen) and Dr Jèrome Villette for many fruitful discussions. The authors would like to thank Dr C. F. Abrams and Prof. D. B. Graves in whose group the code we have utilized was originally developed.

This work, supported by the European Communities under the Contract of Association between EURATOM/FOM (FOM Programme 55), was carried out within the framework of the European Fusion Programme. The views and opinions expressed herein do not necessarily reflect those of the European Commission.

References

[1] J. A. Bondur, J. Vac. Sci. Technol. **13**, 1023 (1976).
[2] L. A. Brussaard, A. Fasolino, and T. Janssen, Phys. Rev. B **63**, 214302 (2001).
[3] J. P. Chang and J. W. Coburn, J. Vac. Sci. Technol. A **21**, S145 (2003).
[4] T. P. Chow and A. J. Steckl, J. Electrochem. Soc. **131**, 2325 (1984).
[5] J. W. Coburn, Vacuum **38**, 947 (1988).
[6] V. M. Donnelly, D. L. Flamm, and D. E. Ibbotson, J. Vac. Sci. Technol. A **1**, 626 (1983).
[7] H. W. Lehmann, J. Vac. Sci. Technol. B **6**, 1881 (1988).

[8] R. G. Poulsen, J. Vac. Sci. Technol. **14**, 266 (1977).
[9] K. L. Steffens and M. A. Sobolewski, J. Vac. Sci. Technol. A **17**, 517 (1999).
[10] K. L. Steffens and M. A. Sobolewski, J. Appl. Phys. **96**, 71 (2004).
[11] H. F. Winters and J. W. Coburn, Surf. Sci. Rep. **14**, 161 (1992).
[12] K. Yonekura, K. Yoshikawa, Y. Fujiwara, *et al.*, Thin Solid Films **515**, 5012 (2007).
[13] M. J. Barela, H. M. Anderson, and G. S. Oehrlein, J. Vac. Sci. Technol. A **23**, 408 (2005).
[14] J. P. Booth, Pure Appl. Chem. **74**, 397 (2002).
[15] J. P. Booth, Plasma Sources Sci. Technol. **8**, 249 (1999).
[16] J. P. Booth, G. Cunge, F. Neuilly, *et al.*, Plasma Sources Sci. Technol. **7**, 423 (1998).
[17] G. Cunge, M. Kogelschatz, O. Joubert, *et al.*, Plasma Sources Sci. Technol. **14**, S42 (2005).
[18] T. Y. Jung, D. H. Kim, H. B. Lim, *et al.*, Chem. Soc. **27**, 373 (2006).
[19] M. Kogelschatz, G. Cunge, and N. Sadeghi, J. Phys. D: Appl. Phys. **37**, 1954 (2004).
[20] M. Kogelschatz, G. Cunge, and N. Sadeghi, Eur. Phys. J. Appl. Phys. **33**, 205 (2006).
[21] G. Lombardi, K. Hassouni, F. Benedic, *et al.*, J. Appl. Phys. **96**, 6739 (2004).
[22] K. Ono, T. Oomori, M. Tuda, *et al.*, J. Vac. Sci. Technol. A **10**, 1071 (1992).
[23] E. C. Rangel, N. C. da Cruz, M. A. B. de Moraes, *et al.*, Instrum. Meth. B **141**, 211 (1998).
[24] I. P. Vinogradov, A. Dinkelmann, and A. Lunk, J. Phys. D: Appl. Phys. **37**, 3000 (2004).
[25] R. D. Vispute, S. Choopun, R. Enck, *et al.*, J. Electron. Mater. **28**, 275 (1999).
[26] G. S. Oehrlein, J. Vac. Sci. Technol. A **11**, 34 (1993).
[27] Y. Tezuka, N. Kitano, and N. Nakano, J. Electrochem. Soc. **142**, 3569 (1995).
[28] C. Hohle, N. Heckmann, M. Sebald, *et al.*, J. Microlith. Microfab. **4**, 043009 (2005).
[29] I. T. Martin, G. S. Malkov, C. I. Butoi, *et al.*, J. Vac. Sci. Technol. A **22**, 227 (2004).
[30] C. F. Abrams and D. B. Graves, J. Vac. Sci. Technol. A **19**, 175 (2001).
[31] C. F. Abrams and D. B. Graves, Thin Solid Films **374**, 150 (2000).
[32] C. F. Abrams and D. B. Graves, J. Vac. Sci. Technol. A **16**, 3006 (1998).
[33] C. F. Abrams and D. B. Graves, J. Appl. Phys. **86**, 5938 (1999).
[34] C. F. Abrams and D. B. Graves, J. Appl. Phys. **88**, 3734 (2000).
[35] M. E. Barone and D. B. Graves, J. Appl. Phys. **77**, 1263 (1995).
[36] D. W. Brenner, Phys. Rev. B **42**, 9458 (1990).
[37] F. Gou, M. A. Gleeson, and A. W. Kleyn, Phys. Chem. Chem. Phys. **8**, 5522 (2006).
[38] B. A. Helmer and D. B. Graves, J. Vac. Sci. Technol. A **15**, 2252 (1997).
[39] D. Humbird and D. B. Graves, J. Appl. Phys. **96**, 791 (2004).
[40] I. K. Jang and S. B. Sinnott, J. Phys. Chem. B **108**, 18993 (2004).
[41] L. W. Keri, I. B. Carmen, and R. F. Ellen, J. Vac. Sci. Technol. A **21**, 1688 (2003).
[42] M. G. Luca, H. L. Jan, A. Fasolino, *et al.*, Phys. Rev. B **72**, 214103 (2005).
[43] C. Carbogno, A. Gross, and M. Rohlfing, Appl. Phys. A – Mater. **88**, 579 (2007).
[44] A. Gross, A. Eichler, J. Hafner, *et al.*, Surf. Sci. **539**, L542 (2003).
[45] A. Gross, Surf. Sci. **500**, 347 (2002).
[46] M. Lischka and A. Gross, Phys. Rev. B **65**, 075420 (2002).
[47] A. Gross, Phys. Status Solidi B **217**, 389 (2000).
[48] A. Gross, Surf. Sci. Rep. **32**, 291 (1998).
[49] T. Ezaki and T. Ohno, Jpn J. Appl. Phys. **140**, 2115 (2001).
[50] J. R. Engstrom, M. M. Nelson, and T. Engel, Surf. Sci. **215**, 437 (1989).
[51] K. Sasata, T. Yokosuka, H. Kurokawa, *et al.*, Jpn J. Appl. Phys. **142**, 1859 (2003).
[52] P. Ho, J. E. Johannes, R. J. Buss, *et al.*, J. Vac. Sci. Technol. A **19**, 2344 (2001).
[53] C. Kohler and T. Frauenheim, Surf. Sci. **600**, 453 (2006).
[54] S. D. Athavale and D. J. Economou, J. Vac. Sci. Technol. A **13**, 966 (1995).
[55] F. Gou, M. A. Gleeson, J. Villette, *et al.*, Nucl. Instrum. Meth. B **247**, 244 (2006).
[56] D. B. Graves and D. Humbird, Appl. Surf. Sci. **192**, 72 (2002).
[57] D. Humbird and D. B. Graves, J. Chem. Phys. **120**, 2405 (2004).
[58] D. Humbird and D. B. Graves, J. Appl. Phys. **96**, 2466 (2004).

Downloaded At: 15:50 21 January 2011

[59] C. T. Reeves, B. A. Ferguson, C. B. Mullins, *et al.*, J. Chem. Phys. **111**, 7567 (1999).
[60] T. A. Schoolcraft, A. M. Diehl, A. B. Steel, *et al.*, J. Vac. Sci. Technol. A **13**, 1861 (1995).
[61] F. Gou, L. Z. T. Chen, C. Meng, *et al.*, Appl. Phys. A – Mater. **88**, 385 (2007).
[62] F. Gou, Z. Chen, and C. Zhiqian, Eur. Phys. J. – Appl. Phys. **38**, 129 (2007).
[63] F. Gou, M. A. Gleeson, and A. W. Kleyn, Surf. Sci. **601**, 4250 (2007).
[64] F. Gou, M. A. Gleeson, and A. W. Kleyn, Surf. Sci. **601**, 3965 (2007).
[65] F. Gou, A. W. Kleyn, and M. A. Gleeson, Nucl. Instrum. Meth. B **258**, 52 (2007).
[66] F. Gou, M. C. Liang, Z. Chen, *et al.*, Appl. Surf. Sci. **253**, 8743 (2007).
[67] F. Gou, C. L. Meng, L. Z. Chen, *et al.*, J. Vac. Sci. Technol. A **25**, 680 (2007).
[68] F. Gou, C. L. Meng, Z. T. Zhouling, *et al.*, Appl. Surf. Sci. **253**, 8517 (2007).
[69] F. Gou, Q. Xie, L. Zhu, *et al.*, Nucl. Instrum. Meth. B **248**, 113 (2006).
[70] F. H. Stillinger and T. A. Weber, Phys. Rev. Lett. **62**, 2144 (1989).
[71] F. H. Stillinger and T. A. Weber, J. Chem. Phys. **88**, 5123 (1988).
[72] J. Tersoff, Phys. Rev. Lett. **61**, 2879 (1988).
[73] J. Tersoff, Phys. Rev. B **38**, 9902 (1988).
[74] J. Tersoff, Phys. Rev. B **39**, 5566 (1989).
[75] J. Tersoff, Phys. Rev. B **37**, 6991 (1988).
[76] J. Tersoff, Phys. Rev. Lett. **56**, 632 (1986).
[77] D. W. Brenner, O. A. Shenderova, J. A. Harrison, *et al.*, J. Phys. C – Condens. Mat. **14**, 783 (2002).
[78] B. J. Garrison and D. Srivastava, Annu. Rev. Phys. Chem. **46**, 373 (1995).
[79] C. F. Abrams and D. B. Graves, J. Vac. Sci. Technol. A **18**, 411 (2000).
[80] C. F. Abrams and D. B. Graves, IEEE Trans. Plasma Sci. **27**, 1426 (1999).
[81] D. Humbird and D. B. Graves, J. Chem. Phys. **120**, 2405 (2004).
[82] J. Tanaka, C. F. Abrams, and D. B. Graves, J. Vac. Sci. Technol. A **18**, 938 (2000).
[83] P. C. Weakliem and E. A. Carter, Abstr. Pap. Am. Chem. Soci. **204**, 4 (1992).
[84] R. L. C. Vink, G. T. Barkema, W. F. van der Weg, *et al.*, J. Non-Cryst. Solids **282**, 248 (2001).
[85] L. Zhang and J. Y. Feng, Nucl. Instrum. Meth. B **234**, 487 (2005).
[86] Y. Kadiri, N. Jakse, J. F. Wax, *et al.*, J. Non-Cryst. Solids **312–314**, 143 (2002).
[87] H. W. Lu, J. Q. Xie, and J. Y. Feng, Nucl. Instrum. Meth. B **170**, 71 (2000).
[88] B. Weber and K. Gartner, Nucl. Instrum. Meth. B **175**, 119 (2001).
[89] P. C. Weakliem, C. J. Wu, and E. A. Carter, Phys. Rev. Lett. **69**, 200 (1992).
[90] P. C. Weakliem and E. A. Carter, J. Chem. Phys. **98**, 737 (1993).
[91] L. E. Carter and E. A. Carter, J. Phys. Chem. **100**, 873 (1996).
[92] F. Gou, M. A. Gleeson, and A. W. Kleyn, Surf. Sci. **601**, 76 (2007).
[93] H. C. Andersen, J. Chem. Phys. **72**, 2384 (1980).
[94] S. Nose, J. Chem. Phys. **81**, 511 (1984).
[95] H. J. C. Berendsen, J. P. M. Postma, W. F. V. Gunsteren, *et al.*, J. Chem. Phys. **81**, 3684 (1984).
[96] P. Erhart and K. Albe, Appl. Surf. Sci. **226**, 12 (2004).
[97] S. Nose and M. L. Klein, Phys. Rev. B **33**, 339 (1986).
[98] S. Nose and M. L. Klein, Phys. Rev. Lett. **53**, 818 (1984).
[99] W. G. Hoover, Phys. Rev. A **31**, 1695 (1985).
[100] W. G. Hoover, Phys. Rev. A **34**, 2499 (1986).
[101] D. Humbird and D. B. Graves, J. Appl. Phys. **96**, 65 (2004).
[102] H. P. Kaukonen and R. M. Nieminen, Phys. Rev. Lett. **68**, 620 (1992).
[103] J. L. Mauer, J. S. Logan, L. B. Zielinski, *et al.*, J. Vac. Sci. Technol. **15**, 1734 (1978).
[104] Y.-Y. Tu, T. J. Chuang, and H. F. Winters, Phys. Rev. B **23**, 823 (1981).
[105] P. G. M. Sebel, L. J. F. Hermans, and H. C. W. Beijerinck, J. Vac. Sci. Technol. A **18**, 2759 (2000).
[106] K. L. Williams and E. R. Fisher, J. Vac. Sci. Technol. A **21**, 1024 (2003).
[107] D. Humbird and D. B. Graves, J. Vac. Sci. Technol. A **23**, 31 (2005).

Downloaded At: 15:50 21 January 2011

[108] D. W. Hess, Annu. Rev. Mater Sci. **16**, 163 (1986).
[109] H. F. Winters and J. W. Coburn, Surf. Sci. Rep. **14**, 161 (1992).
[110] D. L. Flamm, V. M. Donnelly, and D. E. Ibbotson, J. Vac. Sci. Technol. B **1**, 23 (1983).
[111] A. Galijatovic, A. Darcy, B. Acree, *et al*., J. Phys. Chem. **100**, 9471 (1996).
[112] T. A. Schoolcraft and B. J. Garrison, J. Am. Chem. Soc. **113**, 8221 (1991).
[113] G. V. Gadiyak, Y. N. Morokov, and D. N. Mukhin, Appl. Surf. Sci. **60–1**, 131 (1992).
[114] M. J. Vasile and F. A. Stevie, J. Appl. Phys. **53**, 3799 (1982).
[115] G. P. Kota, J. W. Coburn, and D. B. Graves, J. Appl. Phys. **85**, 74 (1999).
[116] F. Greer, D. Fraser, J. W. Coburn, *et al*., J. Appl. Phys. **94**, 7453 (2003).
[117] J. W. Coburn, Pure Appl. Chem. **64**, 709 (1992).
[118] V. M. Bermudez, J. Vac. Sci. Technol. A **10**, 3478 (1992).
[119] A. Darcy, A. Galijatovic, R. Barth, *et al*., J. Mol. Graphics Model. **14**, 260 (1996).
[120] C. W. Lo, P. R. Varekamp, D. K. Shuh, *et al*., Surf. Sci. **292**, 171 (1993).
[121] M. R. Tate, D. Gosalvez-Blanco, D. P. Pullman, *et al*., J. Chem. Phys. **111**, 3679 (1999).
[122] M. R. Tate, D. P. Pullman, Y. L. Li, *et al*., J. Chem. Phys. **112**, 5190 (2000).
[123] C. J. Wu and E. A. Carter, J. Am. Chem. Soc. **113**, 9061 (1991).
[124] C. J. Wu and E. A. Carter, Phys. Rev. B **45**, 9065 (1992).
[125] C. Yang, H. C. Kang, and E. S. Tok, Surf. Sci. **465**, 9 (2000).
[126] K. Ninomiya, K. Suzuki, S. Nishimatsu, *et al*., J. Appl. Phys. **62**, 1459 (1987).
[127] T. Aoki and J. Matsuo, Nucl. Instrum. Meth. B **241**, 594 (2005).
[128] H. Toyoda, H. Morishima, R. Fukute, *et al*., J. Appl. Phys. **95**, 5172 (2004).
[129] T. Sikola, D. G. Armour, and J. A. VandenBerg, J. Vac. Sci. Technol. A **14**, 3156 (1996).
[130] J. W. Coburn, H. F. Winters, and T. J. Chuang, J. Appl. Phys. **48**, 3532 (1977).
[131] J. W. Coburn, Appl. Phys. A – Mater. **59**, 451 (1994).
[132] J. J. Vegh, D. Humbird, and D. B. Graves, J. Vac. Sci. Technol. A **23**, 1598 (2005).
[133] F. Gou, A. W. Kleyn, M. A. Gleeson, In preparation.

Downloaded At: 15:50 21 January 2011